Final Report

Towards Smart Grid Ready SOFC

(ForskEL project no. 2012-1-10747)

Johan Hjelm

July 30, 2014

Contributing Authors:

Johan Hjelm[1], Christopher Graves[1], Anne Hauch[1], Jean-Claude Njodzefon[1], Xiufu Sun[1], Tania Ramos[1], Sune Veltzé[1], Karin Vels Hansen[1], Karen Brodersen[1], Dino Boccaccini[1], Rasmus Mosbæk[1], Peter Stanley Jørgensen[1], Karl Thyden[1], Søren Bredmose Simonsen[1], Søren Højgaard Jensen[1], Christophe Gadea[1], Qiang Hu[1], Vincenzo Esposito[1], Martin Søgaard[1], Mogens Mogensen[1], Anke Hagen[1], Theis Løye Skafte[1,2], Per Hjalmarsson[1,2], Jesper Noes[2], Christian Bang-Møller[2], Peter Blennow[2], Steen Weichel[2], Rasmus Barfod[2], Sif Kjølby[2], Laila Grahl Madsen[3], Bertil Sieborg[3]

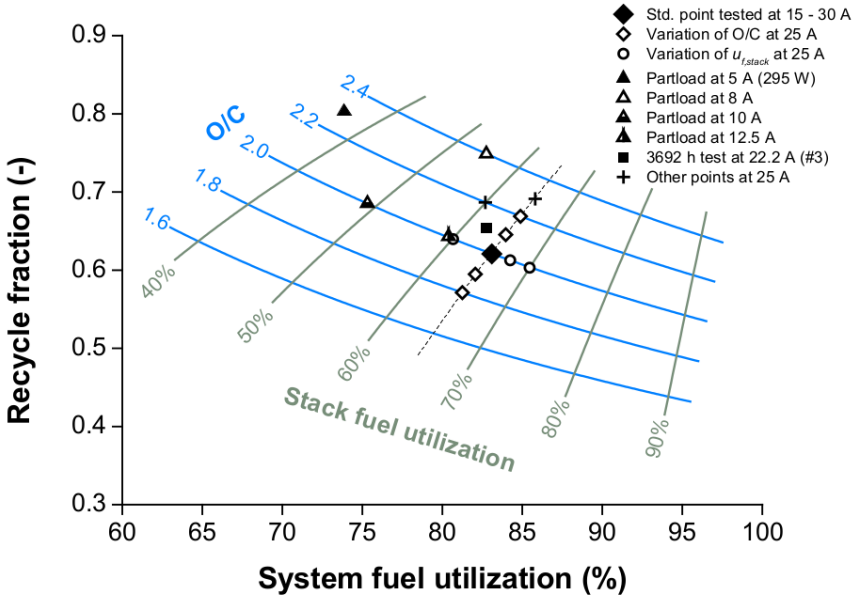

Affiliations:

1. DTU Energy Conversion, Risø Campus, Frederiksborgvej 399, DK-4000, Roskilde, Denmark
2. Topsoe Fuel Cells A/S, Nymøllevej 66, DK-2800 Kgs. Lyngby, Denmark
3. IRD Fuel Cell A/S, Kullinggade 31, DK-5700 Svendborg, Denmark

Contents

1 Final Report

1.1 Project Details

Project title	Towards Smart Grid Ready SOFC
Project identification	Energinet.dk project no. 2012-1-10747
Name of the programme which has funded the project	ForskEL
Name and address of the enterprises/institution responsible for the project	Department of Energy Conversion and Storage, Technical University of Denmark, Frederiksborgvej 399, DK-4000, Roskilde
CVR (central business register)	30060946
Date for submission	31-July-2014

1.2 Executive Summary

The solid oxide fuel cell can deliver power and heat from natural gas or biogas with high electrical efficiency and low distribution losses. This can for example be utilised in distributed generation or combined heat and power in district heating grids or as micro combined heat and power (mCHP) in domestic housing. Solid oxide fuel cell systems for CHP/DG applications can be supplied with fuel from the national gas grid. In the process of becoming fossil free, the natural gas in the grid could gradually be substituted by biogas or synthetic gas made in bio-refineries or by electrolysis. The gas grid can store large amounts of energy and is thus an important backbone in the vision of a flexible energy system in Denmark with inherently fluctuating wind power as major source of electricity. However, this requires that the SOFC systems used as energy conversion units for natural gas, bio gas, landfill gas or hydrogen can be controlled in a way to follow the changing demands for power.

Making an SOFC based CHP system ready for Smart Grid applications requires effort in research and development on many levels: from the relatively fundamental research involved in identification of critical issues at the cell level, increasing understanding of performance and lifetime limiting effects, continuing development of new cell generations with better performance and greater robustness at DTU Energy Conversion, testing and mapping of the dynamic capabilities of the current stack technologies at Topsoe Fuel Cell, to the actual implementation of the SOFC systems into complete CHP units developed by system integrators.

The work packages are listed below along with the different sub tasks that were defined in the project application:

- WP1 - Smart Grid Requirements & Capabilities of SOFC
- WP2 - Auxiliary Components
- WP3 - Single Cell Testing
- WP4 - Stack Mapping and Testing
- WP5 - Mechanical Properties of Critical Interfaces and Layers
- WP6 - Cell Components

WP1 started out by analysing possible demands on a SOFC system operating in a smart grid context. Suggestions for test objectives and specific tests to demonstrate the smart grid readiness of the technology were made and picked up in WP4 where the stack and PowerCore testing was carried out. Based on the outcome of the analysis in WP1 a few different gas compositions were selected also for

testing of single cells in WP3. A database was also created with categorized and prioritized degradation processes / lifetime limiting effects.

WP2 was charged with the task of carrying out auxiliary component testing which in this case translated to testing of glass-based sealant gaskets as a function of time under thermal load and as a function of thermal cycling. A modified test fixture was designed and used for the testing.

All single cell testing and related activities were carried out in WP3. A modified test fixture was developed for single cell testing that yielded improvements in test turnover, accuracy, and reproducibility. The new test fixture further makes a greater range of start-up temperatures for cell tests available, and it was shown that it is possible to test cells that have been reduced ex-situ, prior to testing, which may be a useful tool for future investigations of surface modifed Ni-cermet electrodes in full cells. In order to utilize the test results a large body of work was carried out in the area of data analysis, interpretation in terms of physical models yielding a closer connection between the quantified parameters and materials and structural parameters, and data visualization. A large part of the experimental work carried out was focused on detailed investigations of cell performance in various carbonaceous fuels (e.g. methane reformate). The stability of cells exposed to sulfur containing fuel gas was also further explored.

WP4 took care of all stack and PowerCore testing and performance mapping. Various operating modes (idling, power burst/max load, nominal load) of stacks were explored, and the different operating points mapped also in PowerCores. Significant advances in diagnostic methodology were made exemplified by successful spatially resolved temperature measurements and detailed impedance investigations of operating stacks. The impedance based diagnostic effort lead to a demonstration of the possibility of investigating the average cell temperature profile and fuel flow distribution in a short (14 cell) stack. Towards the end of a project the outcome of a recent smaller stack production campaign was evaluated and found to produce highly satisfactory results.

WP5 had the challenging task of attempting to investigate mechanical properties of critical interfaces and layers in SOFCs and repeating units in stacks (interconnects + cell). Sample preparation and identification of suitable methods consumed much of the effort in this work package at the beginning of the project, but was successful in identifying critical interfaces, and also quantified mechanical properties of materials in the porous electrodes, the dense electrolyte, and could provide new information on the mechanical properties of interfaces between the functional layers in the cell and between interconnect plates and cells.

WP6 developed and produced a number of series of cells using mainly tape-casting, but a cell with a very thin electrolyte produced using ink-jet printing was also investigated in the project. The efforts in WP6 lead to the development of cells with improved performance by decrease of the electrolyte thickness and by preparation of an improved anode. Methodology for investigation of fundamental interactions between the nickel phase and the ceramic phase in Ni-cermet electrodes was also developed.

Listed below are the milestones that were defined for the project and their status at completion of the project:

1. M1.1 - Definition of Test Profiles and Key Operating Points
   An analysis of the Smart Grid requirements for SOFC was carried out in the beginning of the project. This analysis lead to the suggestion of a number of tests to be carried out to evaluate the capability of SOFC technology to meet expected needs of a SOFC system integrated in a Smart Grid context. For single cell testing two main gas compositions were selected for durability testing. The milestone is considered fulfilled.

2. M1.2 - Documentation of Smart Grid Demands and Capabilities of SOFC Technology
   During the project it was shown that the overall characteristics of the SOFC technology in this project is quite relevant for Smart Grid applications and that the technology is capable of following the dynamic load changes. However, it has also been evident that the biggest issues before successfully implementing the SOFC technology in Smart Grid systems is more on the fundamental improvement of lifetime and robustness. The business case for implementing SOFC technology in Smart Grids either as mCHP or larger Distributed Generation units shows that the lifetime must be increased further from the current state-of-the-art. The milestone is considered fulfilled.

3. M2.1 - Durability of at least two different sealants tested as a function of thermal cycles
   Two different sealant gasket types, one with screen-printed glass paste on either side of a stainless steel frame, and one glass only gasket, were characterized with respect to leak tightness as a function of thermal cycles. The milestone is considered fulfilled.

4. M3.1 - A comparison of the overvoltage – current characteristics of at least two different Ni-cermet anodes in reformate gas completed

Three different cells were investigated in hydrogen - steam fuel mixtures along with two different carbonaceous fuel mixtures, and process specific overpotential - current curves were constructed from the collected impedance data. The milestone is considered fulfilled.

5. M3.2 - Quantification of the long-term degradation rate of cells with at least two different Ni-cermet anodes in reformate gas
   Two different cells were subjected to ~1000 h long durability tests at 0.5 A cm^{-2} in internally reformed methane fuel. Further exploration of the durability during the first 1000 h of operation in three different fuel compositions were undertaken for one of the cell types. Further work including longer tests and repeat tests are necessary to provide a reliable long-term degradation rate. As it is not clear at present whether 1000 h test periods are sufficient to assess the long-term degradation rate for cells operating in methane reformate fuel, the milestone is considered partially fulfilled.

6. M4.1 - Mapping experiments conducted on at least 3 stacks
   More than ten stacks were tested and a number of tests covering most of the tests goals suggested in WP1 were carried out. Further evaluation of electrical efficiency as a function of fuel utilization, anode recycle fraction, and gas composition was carried out on PowerCores. The milestone is considered fulfilled.

7. M4.2 - Demonstrate improved robustness of stack towards loss of electrical contact
   A production campaign (funded by another project) was carried out, in which selected stack improvements (developed in this and other projects) were implemented, and the resulting 28 stacks were subsequently subjected to a quality assurance test including a harsh robustness test. None of the tested stacks were rejected in the quality control. No serious robustness issues were discovered by the extended robustness test, and the campaign adds significantly to the confidence in the chosen and implemented stack improvements. It also confirms that the milestone has been fulfilled.

8. M4.3 - Establishment of electrochemical impedance analysis as a tool for diagnostics of technological stacks
   A new parallel impedance measurement set-up allowing simultaneous acquisition of the stack impedance along with the impedance of up to 16 repeating units or cell blocks was implemented and detailed impedance measurements were carried out on a stack with 14 repeating units. The fuel flow distribution, ohmic resistance, and information illustrating the average cell temperature distribution from top to bottom in the stack was obtained from these measurements. The milestone is considered fulfilled.

9. M5.1 – Quantification of the adhesion and cohesion of two different cathode-side layers completed
   A series of samples of differently sintered LSC-CGO cathodes were investigated using nanoindentation. The interfacial mechanical properties of three different interconnect - cathode side layer samples were investigated and a measure of adhesion, the failure load, obtained using three-point bending tests. The milestone is considered fulfilled.

10. M5.2 - Quantification of the anode-side (anode / interconnect) adhesion completed
    The same experimental approach employed for the assessment of bonding strength in cathodes was applied to study the anode-interconnect interface. The anode-interconnect interface was found to exhbit a significantly stronger adhesion than the different cathode - interconnect interfaces investigated. The fracture toughness of the anode support material (Ni-3YSZ) was found to be greater than the interfacial toughness between anode support and metal interconnect. The milestone is considered fulfilled.

11. M6.1 - A cell with physically more robust cathode layers developed and delivered for testing
    The work on increased robustness cathodes was reduced to a smaller effort in the project, as the work in WP5 indicated that cathode – interconnect interface is a much weaker interface than the cathode – barrier layer interface is. A series of cells with LSC-CGO cathodes of varying microstructure was produced and delivered for testing. Milestone M6.1 is therefore considered not fulfilled: although the samples made provided a possibility to evaluate variations in cohesion in such a cathode, no actual full cell with an improved physical robustness was delivered for testing in the project.

12. M6.2 An improved cell developed and delivered for testing
    Tape-cast and laminated anode-supported cells were developed with 4-6 µm thin YSZ electrolytes. An anode layer with reduced particle size was developed and delivered for testing. These improvements were integrated in a cell that delivered for testing. In conjunction with another project an

anode supported cell was with a ~1.2 µm thick electrolyte was manufactured using ink-jet printing. A series of cells with barrier layers of different thickness were investigated. The milestone is considered fulfilled.

1.3 Project Results

So far the development of the SOFC systems in Denmark has focused on the steady base load use, where significant R&D is still needed to match the market requirements with respect to performance, reliability, and price. In the project "Durable and Robust SOFC" [ForskEl project # 2010-1-10441] focus was placed on constant load operation of the improved 2nd generation cells, with new, improved cathodes based on mixed electronic and ionic conductor (MIEC) materials such as $La_{1-x}Sr_xCoO_{3-\delta}$, (LSC), and $La_{1-x}Sr_xCo_{1-y}Fe_yO_{3-\delta}$, (LSCF) with most of the testing carried out with hydrogen as fuel. The main objectives of "Durable and Robust SOFC" were cells with better performance, improved durability, and greater chemical and physical robustness. This project continued to pursue these goals, with targets firmly anchored in the national road map for SOFC implementation, but moved the focus on to make SOFCs more ready for integration in a Smart Grid. Specifically, this project addressed the following issues:

- Identification and mapping of those Smart Grid operating conditions relevant for SOFC
- Durability and robustness under dynamic operating conditions to cope with fluctuating electricity demand
- Investigations of performance and stability in methane reformate fuels

The expected outcome of the project can be summarized as follows:

- Definition of Smart Grid relevant conditions and their translation to single cell operation specifications, including expected normal operation and extreme conditions
- Development of necessary testing methodology that allows for accurate and detailed characterization of SOFCs under relevant operating conditions
- Mapping of SOFC performance and durability under the identified smart grid conditions, including use of carbon containing fuels with relevant impurities, both on state-of-the-art and improved cells
- Identification of possible performance and lifetime limiting effects caused by dynamic operating conditions at the stack level
- Improved understanding of losses associated with operation in methane based fuels (gas mixtures with compositions corresponding to natural gas / biogas / landfill gas)
- Understanding of critical issues for smart grid operation of single cells related to: 1) Stability of critical interfaces in the cell 2) Fracture strength and toughness of key cell components (in particular the weaker cathode side layers) 3) Use of this understanding to improve the cells for smart grid applications.
- Improvement of cell components to advance Danish SOFC technology further towards the goals set out in the national implementation plan.

The points listed above were to a large extent covered by the project activities and key results are summarized in the following.

1.3.1 WP1 - Smart Grid Requirements & Capabilities

An analysis of the Smart Grid requirements for SOFC was carried out in the beginning of the project. It was shown that the load profiles for heat and power for a household would call for a very dynamic operation of the SOFC system unless a significant heat buffer is in place and that the electricity production could use the grid as a buffer. However, with a significant heat buffer, the power production can be detached from the current heat demand of the individual house, and the SOFC power plant will thus be a possible tool for regulating the grid power production by making each small SOFC unit part of a Virtual Power Plant, which can then be controllable for regulating the power.

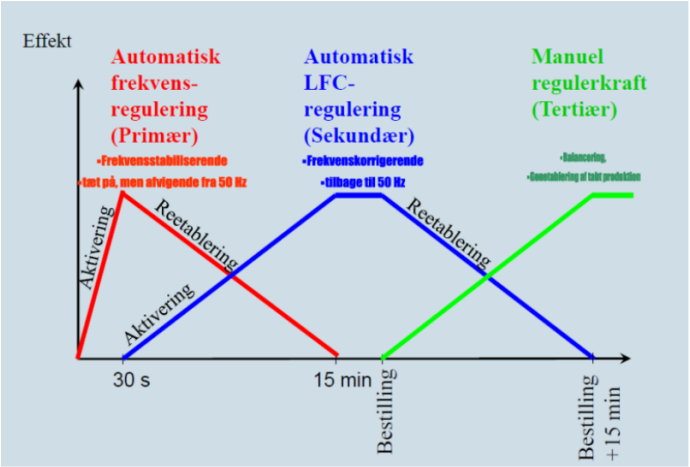

Figure 1: Grid regulation services

For grid regulation three domains of response times from power generators are defined as in figure 1. The interim report "Mapping of Fuel Cell operating points" describes how TOFC in the project have tested load cycles on SOFC stacks with changes in the order of 100W/s. This enables the SOFC system to act as a primary frequency regulation within 5 seconds as shown in the chart above. It is therefore shown that SOFC systems can be used as one of the tools for the most important primary frequency regulation. However, with the high efficiency and when connected to a sufficient heat buffer, an SOFC CHP system is also fully capable of supporting the secondary or tertiary regulation domains as well.

Household microCHP systems or larger Distributed Generation systems based on the Topsoe Fuel Cell SOFC technology could also fit nicely into the Smart Grid concept envisioned in the EU EcoGrid project (http://www.eu-ecogrid.net/). Here a large scale demonstration of Smart Grid technologies is being implemented on the island of Bornholm with amongst others DTU as a partner. In the EcoGrid concept the regulation is based on a "real-time" price signal. So instead of connecting the individual smaller units into a larger "Virtual Power Plant", the individual units will have built-in logics to decide on the operating point based on the current market price. In this way an SOFC mCHP unit can choose to increase the power production when the price is high – even if the momentary household consumption is low. The price will change every five minutes, which is much longer than the minimum response time of the SOFC units which is in seconds.

1.3.1.1 Operating Points In order for the SOFC system to contribute to grid regulation it must be able to handle different operating points. In the application of this project we showed the following schematics on how an operating map of an SOFC system could look like. These operating modes are illustrated in Figure 2.

Figure 2 is originally from the application of this project, but here a couple of additional operating modes have been included. The operating modes are also listed in Table 1 together with suggested goals and tests.

Operating mode	Suggested goal	Suggested test
Power burst	0.23 A/cm^2 to 0.5 A/cm^{2}in 5 s and back in 15 min	Power burst cycles (at constant FU)
Max power	0.5 A/cm^2 in 2 h	Max power cycles (at constant FU)
Transient response (up)	10-90% load in 2 min	Load cycles (at constant FU)
Transient response (down)	90-10% load in 2 min	(tested when testing "Transient response (up)")
Idle (no power export)	10% load in 12 h (load corresponds to parasitic loss)	10% load in 12 h (at low FU)
Cold start-up	Start-up in 30 min	Stack start-up test with max heat-up rate
(Max heat)	(no goal)	(not relevant if separate burner is installed)

Table 1: List of suggested goals and tests for the relevant operating modes. FU is fuel utilization.

In the project report "Mapping of Fuel Cell operating points" we have shown how we could test some

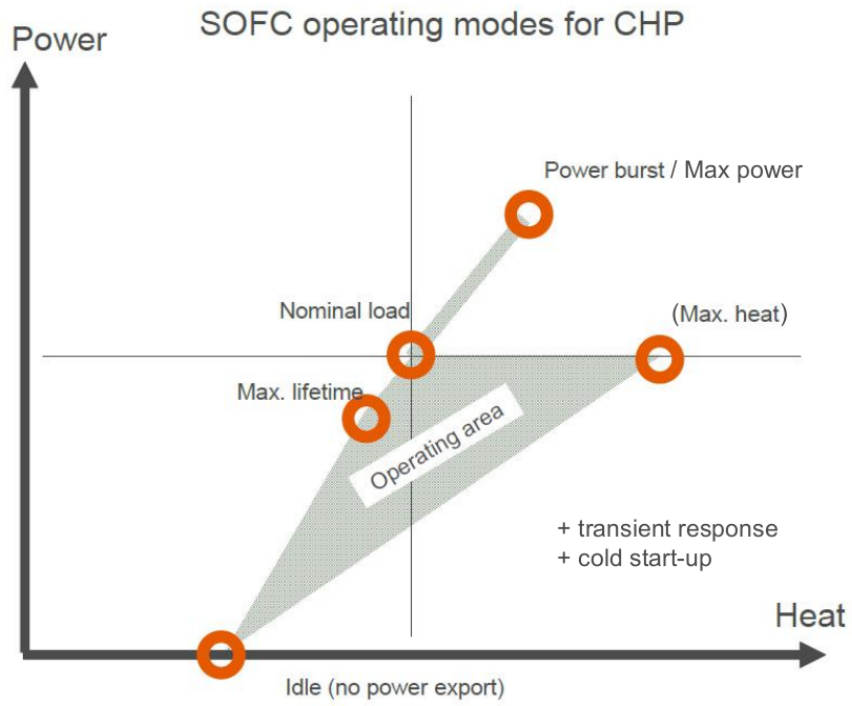

Figure 2: Schematic view of possible operating modes for a Smart Grid ready SOFC CHP system.

of these points and the dynamic capabilities. Many of the tests have been made the TOFC "PowerCore" system (SOFC stack including BoP components) which is more system relevant than stack tests. We have shown that the "Power burst" point is possible, but that the efficiency is drastically lowered. We have not shown whether the "Max. lifetime" operating point is different from our "Nominal load" point, but extensive work on understanding and improving lifetime has been done in this project and in other projects.

The operating points can also be illustrated in the following way (figure 3) which better depicts the derived operating parameters Fuel Utilization, anode recycle ratio and system fuel utilization, which are important parameters when deciding on an operating point.

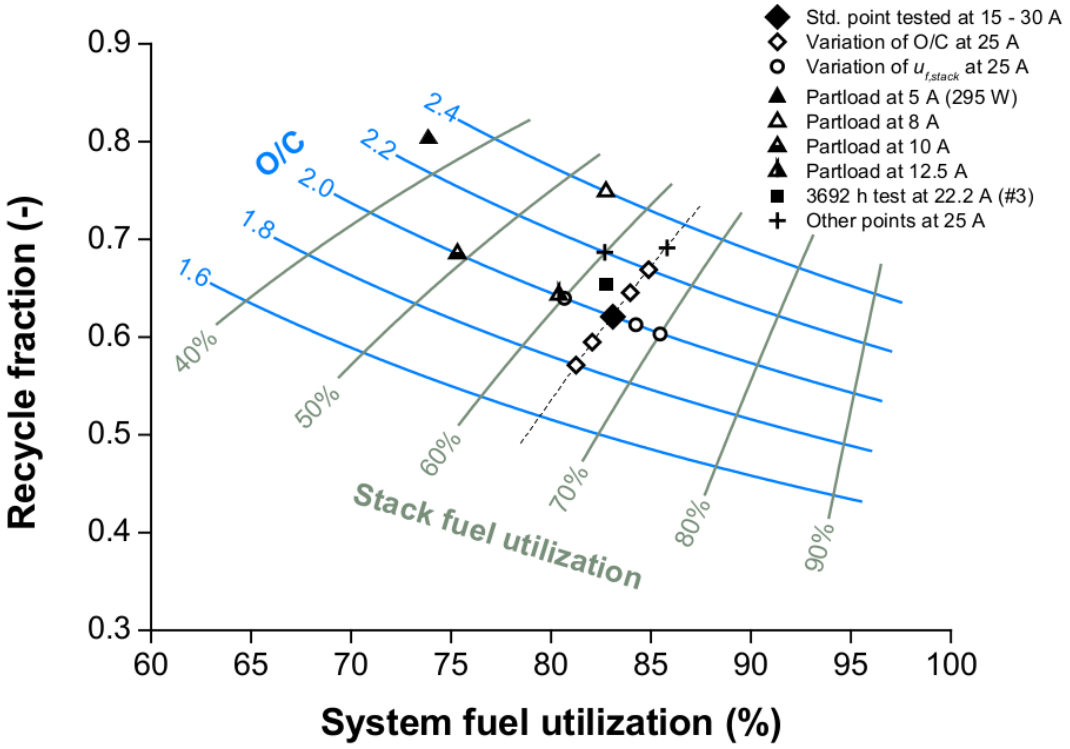

Figure 3: Mapping of the operating points in recycle system domain with reformate fuel.

The chart shows how we have mapped the performance of the system in various points, and specifically from a load range from 5 A to 30 A (nominal load is 25 A). This corresponds to varying the power output from "Idle" to "Power burst" in figure 2. (Some of the work described here has been performed under the EUDP project "SOFC Accelerated" ENS-64012-0225)

The results are encouraging for Smart Grid application and shows the strength of the SOFC technology for load following.

In figure 4 the DC efficiency (excluding auxiliary power loss and inverter power loss) is shown over the complete operating range from 5 A to 30 A. It should be noted that unlike most other competing technologies such as internal combustion engines the efficiency of an SOFC system is even higher at part load operation (peak here is at about 17 A).

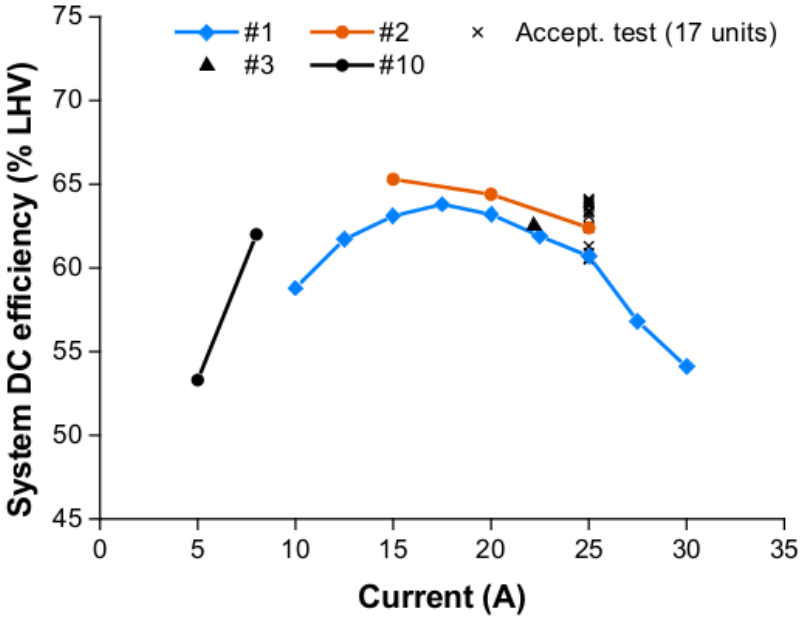

Figure 4: Efficiency of an SOFC system (PowerCore) at varying load

1.3.1.2 Idle Operation In order for the SOFC system to be efficient in a Smart Grid application it needs to be kept hot and in operation, because the heat up of an SOFC system from ambient temperature to the operating temperature of ~750°C consumes energy, takes at least 30 minutes and is also detrimental for the lifetime of the stack. It is thus not expected to start and stop the SOFC system more than 5-10 times per year. In a Smart Grid application there will be periods where the need for power output is small and so the idling performance is important.

During the investigations under this project new ideas have arisen on how to perform the idle operation. By allowing lowering the operating temperature of the stack considerably below the nominal temperature of 750°C the internal resistance of the cells increase considerably. Usually this is an unwanted effect because it lowers the electrical efficiency of the system. However, there are some advantages of doing this if the power export is to be minimized while keeping the system idling. By lowering the temperature the increased internal resistance helps keeping the heat generation where it is needed – inside the stack. Furthermore, by lowering the temperature during idling, the heat losses are minimized and thus the energy to maintain the temperature is minimized. Additionally, the lifetime of the stack components are increased at lower temperatures, but still the power production can be at the nominal operating point within a few minutes.

As a direct result of this project a patent has been filed on this "cold idle" strategy and the ways of implementing it. "Cold Idle Operation of SOFC System" European application no. 14171742.1.

1.3.1.3 WP1 - Conclusion During the project it has been shown that the overall characteristics of the SOFC technology in this project is quite relevant for Smart Grid applications and that the technology is capable of following the dynamic load changes. However, it has also been evident that the biggest issues before successfully implementing the SOFC technology in Smart Grid systems is more on the fundamental improvement of lifetime and robustness. The business case for implementing SOFC technology in Smart Grids either as mCHP or larger Distributed Generation units shows that the lifetime must be increased further from the current state-of-the-art. This is also the reason why much of the effort by TOFC in this project has been refocused on understanding the fundamental lifetime limiting factors and increasing test capabilities on cell level. This is further elaborated on in 1.3.4

1.3.1.4 A Dynamic Database for Degradation and Lifetime Limiting Issues TOFC has a need for improved internal understanding and traceable documentation of degradation mechanisms in all aspects of our product, as well as a need for evaluation of the relevance of known lifetime limiting phenomena in TOFC stacks under the main intended operating conditions. During the last six months of this project TOFC has worked towards solutions to facilitate the identification, characterization, and quantification of lifetime limiting mechanisms using literature, component tests, physical characterization and stack post mortem analysis. The gained knowledge should be established in a retrievable,

generally accessible form, so that TOFC can improve the way it prioritizes lifetime investigations, documentation and improvements. The aim is to make sure that we have a consistent view of the lifetime situation in our current product and that of upcoming solutions. The vision is to know the sources, modes and mechanisms that dominate the lifetime limitations of TOFC's stacks, and to develop tools to conduct lifetime trend prediction of components, cells, and eventually stacks. During 2014 significant progress has been made in adding to and categorizing entries in the "*Degradation Mechanisms Database*". This database will be improved continously, also in subsequent projects, such as SOFC4RET. [ForskEL project no 2014-1-12231].

1.3.2 WP2 - Auxiliary Components

This work package focused on characterization of the leak tightness of various glass sealant gaskets for sealing of SOFC stacks and was organized in a single work task ("WT2.1 - Durability of Sealants during Dynamic Thermal Operating Conditions"). The main focus was investigations of long-term stability of the leak tightness at constant thermal load and when subjected to thermal cycles. A new test fixture was constructed using a steel (Crofer) with a coefficient of thermal expansion (CTE) similar to the cells in a stack was developed in the project in which circular sealing gaskets and combinations of stack components and sealing gaskets could be tested. The leak tightness was evaluated using time-resolved differential pressure measurements. A single milestone was defined for this work package: "Milestone M2.1 Durability of at least two different sealants tested as a function of thermal cycles". The reported results are part of a test matrix defined in close collaboration between TOFC, DTU Energy Conversion, and IRD. The experimental leak tests are performed by IRD, the post test characterization was carried out by TOFC. Two main types of sealing gaskets were investigated:

1. A circular Crofer steel frame with screen-printed glass paste on either side has been tested in a Crofer steel test fixture. The sample was exposed to an aging in air of in total 456 hours at 901±6°C excluding the three thermal cycles of which one cycle was down to RT and two cycles down to 300°C. The measured permeability compares well with the previously reported permeabilities for this gasket and not significantly influenced by controlled thermal cycles nor aging in air. [1]
2. A State-of-the-Art (SoA) SOFC stack glass sealant gasket (Gasket A) has been long term tested towards an anode support in air and exposed to in total eight (8) thermal cycles between 650°C and < 200°C. The total aging time in air was 1234 h at 650°C and 650 h at 750°C, after which time the anode support was reduced. The results show that the gasket performs extremely well in air (5). The initial permeability is significant lower than permeability after the first thermal cycle. However, no changes are recorded after the first thermal cycles, and the air tightness is very good in all tests. The anode support was finally reduced and leakage tested in hydrogen. The tightness was significantly reduced after the Ni-reduction, but the exact permeability cannot be calculated as the mass-flow-controller failed to be exact. A rough estimate of the hydrogen permeability of the sandwich consisting of the SoA SOFC gasket on either side of a reduced anode support is 10^{-8} m^2, which implies unsatisfactorily sealing. Another SoA SOFC stack gasket (Gasket B), which is of a greater thickness than Gasket A, has been tested towards the anode support in an identical manner as Gasket A. The Gasket B / anode support / Gasket B sandwich was too leaktight in air to be characterized with the present test set-up ($<10^{-20}$ m^2). The sample was after sealing and a leak test in air reduced and aged in hydrogen (Fig. 6). The measured permeability in hydrogen for the Gasket B / Anode Support / Gasket B 'sandwich' is in the same order of magnitude as the air permeability for the corresponding Gasket A 'sandwich' in air (Fig. 5). The leakage rate has not been affected by the three thermal cycles nor the long term aging. The tightness of Gasket B is encouraging and of the same order of magnitude as targeted in LT PEMFC stacks.

[1] Sieborg, B & Grahl-Madsen, L (2012): M3.1 Report: Evaluation of three different sealant materials as a function of temperature completed. Confidential Project Report: "Durable and Robust Solid Oxide Fuel Cells" (Energinet.dk, ForskEL project no. 2010-1-10441)

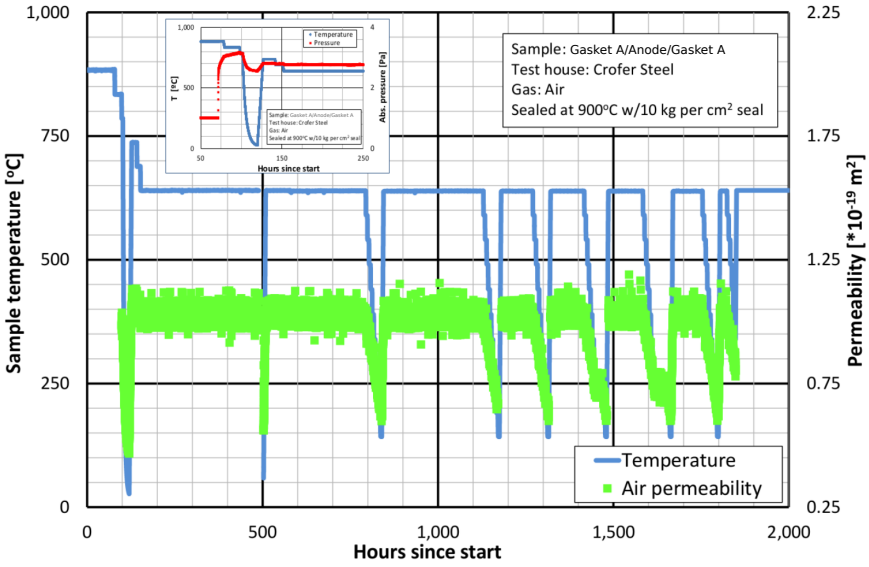

Figure 5: Experimental results of the long-term permeability test of Gasket A on either side of an anode support layer in its oxidized state (NiO-YSZ).

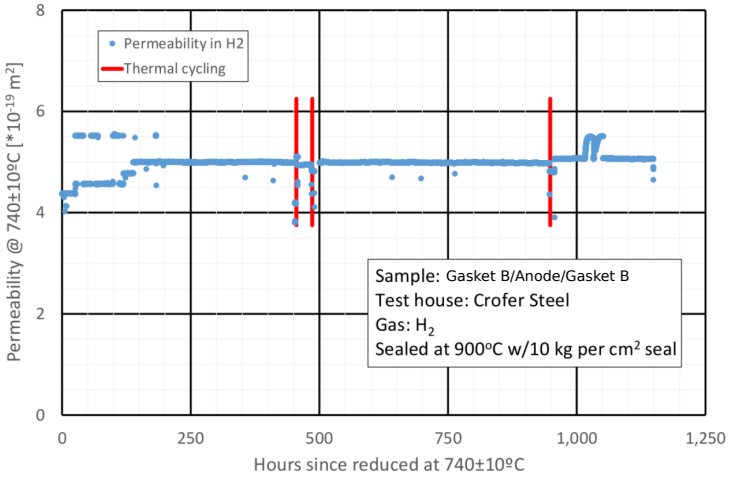

Figure 6: Experimental results of the long-term permeability test of Gasket B on either side of an anode support layer in its reduced (and thus more porous) state (Ni-YSZ).

In conclusion, the work carried out in WP2 has shown that thermal cycling of selected glass sealant gaskets in contact with Crofer steel and/or anode support is not affecting the leak tightness significantly, and that the use of a slightly thicker glass sealant gasket (Gasket B) may be necessary on the anode side. The long-term tests carried out further indicated no significant degradation of the seal quality with time.

1.3.3 WP3 - Single Cell Testing

1.3.3.1 Development of an Improved Solid Oxide Cell Test Fixture A modified test fixture was developed in the project in order to improve test reproducibility and to allow a greater test turnover. By moving to a test fixture design with a two-part oxygen side alumina block, consisting of a frame to hold the cell down onto the anode side sealant gasket, and a oxygen electrode contact block that moves independently of the frame, we obtained a seal-less cathode compartment, and introduced gold foil sealant gaskets on the anode side. It is also possible to use glass sealant gaskets in the test fixture when needed. By removing the glass sealant mounting and dismounting of cells is quicker, and the separate cathode contact block improves reproducibility with respect to contacting. It was shown that a stable contact to the cell was achieved throughout multiple temperature ramps between 850 and 650 ºC. Calculations were carried out to determine the minimum needed electrode/current collector layer conductivity in order to reduce the measurement error to negligible levels.

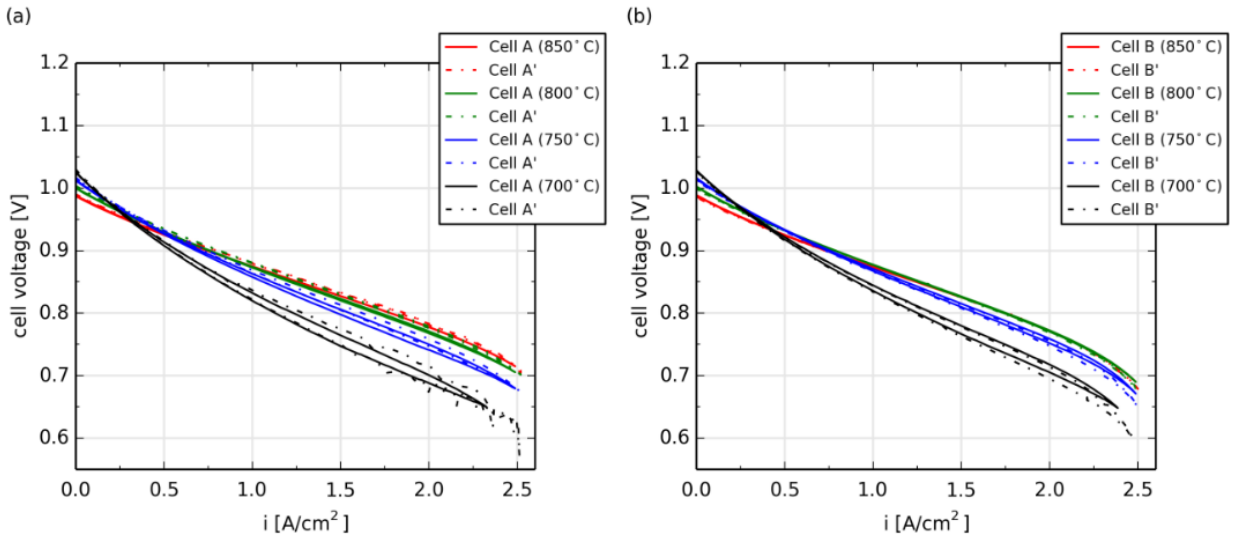

Figure 7: Current - voltage characteristics in the temperature range 700 °C – 850 °C with 20% H_2O at the fuel electrode (25 l/h total fuel mixture flow rate, H_2 balance) and air (140 l/h) at the oxygen electrode for (a) cell A and a sister cell A' and (b) cell b and a sister cell B'. Cells A' and B' were tested at different test-rigs to cells A and B respectively, but all tests were carried out in the same type of test fixture.

The reproducibility of test results obtained in the modified test fixture were assessed in a number of tests, and even though a comprehensive study has not been completed yet, the initial data yields satisfactory results. Figures 7a and b display current-voltage characteristics at different temperatures and 20 % H_2O and 80% H_2 at the fuel electrode for cells A and B respectively (see table 2), compared to their corresponding sister cells tested at a different test-rig 3. The figures illustrate the excellent reproducibility of cell performance between tests of pairs of sister cells (cells from the same production batch), and assuming the cells are highly reproducible, this indicates good reproducibility in terms of contacting/current collection in the test series. Another benefit with the new test fixture is the possibility to with ease introduce new contact components / flow-fields on both side of the cell, and the possibility to test cells with a cathode with a smaller active area.

1.3.3.2 WT3.1 – Impact of Impurities on Electrode Durability The work in this subtask concentrated on i) investigations of sulphur poisoning of the Ni-cermet anode as a function of various key parameters, and ii) explored the potential of a series of nanostructured coatings prepared by infiltration of metal nitrate containing solutions into porous, reduced, Ni-cermets, and subsequent firing of the samples in an oxidizing atmosphere.

1.3.3.2.1 Sulfur Poisoning Studies The work on long-term degradation of SOFC anodes caused by sulfur exposure focused on the influence on the overpotential, and how the overpotential relates to the degradation behavior and any irreversible microstructural changes.

Three sister cells (anode half cells from the same production batch) were tested at 850 °C in a $CH_4/H_2O/H_2$: 30%/60%/10% mixture using a fuel flow rate leading to a fuel utilization of ~50% and then subjected to exposure to 2 ppm H_2S for 500 h. The tests were designed to investigate the effect of anode overpotential on the long-term degradation for Ni/YSZ anodes. The resulting development in the cell voltage over time for the three tests is depicted in Figure 8. The first sulfur test, *YSZ-Low*, was run at 1 A/cm^2, the second sulfur test, *YSZ-Hi*, aimed for a higher overpotential and was operated at 1.38 A/cm^2 and the third test; high overpotential but no sulfur, *YSZ-no-S*, was operated at 1.88 A/cm^2. This test was stepwise decreased in temperature from 850 °C to 790 °C to reach the desired high overpotential. The *YSZ-Hi* test shows a significant and mainly irreversible long-term degradation after the initial loss of performance due to the sulfur exposure.

The left part of figure 9 shows the impedance spectra (Nyquist and Bode plot) recorded before, after 20 h of H_2S exposure, after 500 h of H_2S exposure and after recovery or partly recovery after sulfur exposure for the low overpotential sulfur test, YSZ-Low, and the corresponding spectra recorded during the high overpotential sulfur test, YSZ-Hi, is shown to the right in Figure 9. Lines represent result of equivalent circuit modelling. From the impedance spectra it is evident that the cell performance for the low overpotential YSZ-Low test is almost fully recovered after stopping the H_2S exposure. From

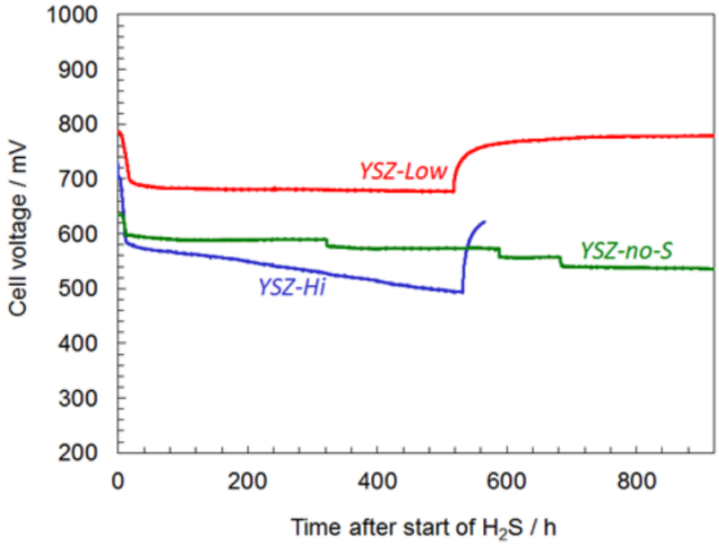

Figure 8: Cell voltage curves as a function of time for H_2S poisoning (2 ppm) at 850 °C, $CH_4/H_2O/H_2$: 30%/60%/10% for YSZ-Low (red), YSZ-Hi (blue) and YSZ-no-S (green). For YSZ-no-S (green) the anode inlet gas composition was H_2/H_2O=80%/20% and no H_2S was added to this test.

the impedance spectra recorded during high overpotential test, YSZ-Hi, it is also clear that for this test there is a significant irreversible increase in the ohmic resistance as well as in the high frequency (above 10 kHz) part of the polarization resistance. During the long-term test of the high overpotential no-sulfur test, YSZ-no-S, both the ohmic resistance and the polarization resistance stayed surprisingly constant. The results from these cell tests, including the analysis of impedance spectra initiated a SEM investigation of the anodes from the three long-term tested cells.

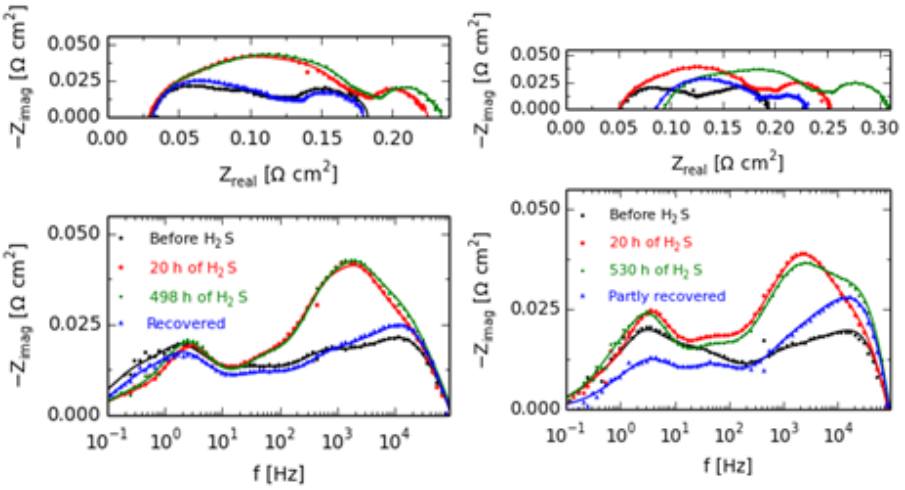

Figure 9: Impedance spectra recorded before, after 20 h of H_2S, after 500 h of H_2S and after recovery or partly recovery after sulfur exposure has ended. The left figure is for the low overpotential sulfur-test, *YSZ-Low*, and the right figure is for the high overpotential sulfur-test, *YSZ-Hi*. All spectra were recorded under current load.

Pieces of the three long-term tested cells were embedded in epoxy and cross-sections were investigated in the SEM. Figure 3 shows representative low-voltage (0.9 kV) in-lens SEM images of the anode/electrolyte interface for the cells from the YSZ-low (low overpotential H_2S test), YSZ-Hi (high overpotential H_2S test) and YSZ-no-S (high overpotential no H_2S test). As described by Thydén et al., the percolating Ni particles will appear bright using this imaging technique[2]. Figure 11 shows representative higher voltage (10 kV) SEM images of the anode/electrolyte interface for the cells from the YSZ-low (low overpotential H_2S test), YSZ-Hi (high overpotential H_2S test) and YSZ-no-S (high overpotential no H_2S test). In these images the epoxy filled pores appear black. From Figure 10 and Figure 11 it is clear that the cell from YSZ-Hi (high overpotential H_2S test) has changed significantly in microstructure and is not comparable to the anodes from the YSZ-low test (low overpotential H_2S test) nor the anode from YSZ-no-S test (high overpotential no H_2S test). For the cell from the YSZ-Hi

[2]K. Thydén, Y. -.L Liu, and J. B. Bilde-Sørensen, Solid State Ionics, 178, 1984 (2008).

test (high overpotential H_2S test) there is a significant lack of percolating Ni particles in the innermost 2-4 µm closest to the electrolyte (Figure 10) and at the same time this anode has an increased pore phase fraction in this same region of the anode, but similar number of pores compared to the anodes from the YSZ-low test (low overpotential H_2S test) and the YSZ-no-S test (high overpotential no H_2S test). In other words, the anode from YSZ-Hi (high overpotential H_2S test) has more of the large pores (indicated using white circles in Figure 11b) when compared to the two other cells; which strongly indicated that these pores are generated in positions in the structure where there used to be Ni particles but where there is now a lack of percolating Ni particles. For quantification of these SEM observations the reader is referred to J. Electrochem. Soc. [3], from which it is also evident that the Ni percolating network and the number of pores and pore phase fractions observed for the YSZ-low test (low overpotential H_2S test) and the YSZ-no-S test (high overpotential no H_2S test) are similar to what has been obtained for a reference cell (non-long-term tested).

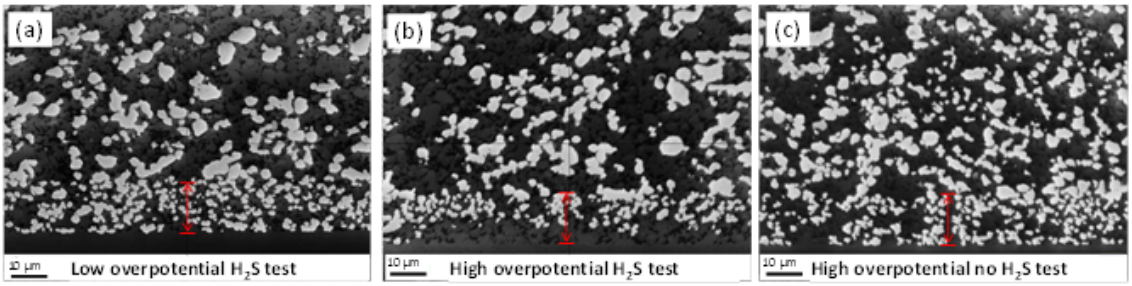

Figure 10: Representative low voltage in-lens SEM images of the anode/electrolyte interface for the cells from the YSZ-low (low overpotential H_2S test), YSZ-Hi (high overpotential H_2S test) and YSZ-no-S (high overpotential no H_2S test). The red bar indicates the thickness of the active anode *i.e.* the lower end of the bar marks the anode/electrolyte interface.

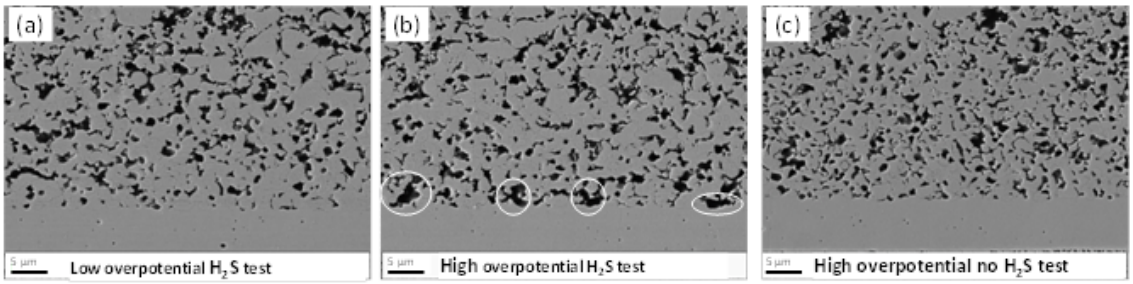

Figure 11: Representative SEM images at an acceleration voltage of 10 kV for polished cross-sections of anode/electrolyte interfaces for the tested cells from (a) YSZ-Low test, (b) YSZ-Hi test and (c) YSZ-no-S test. Circles indicate large porosities in the innermost few microns of the cell from the YSZ-Hi test.

The following summarizes the main findings in this study of the sulfur poisoning of SOFC anodes focusing on the effect of overpotential on long-term degradation and the resulting microstructural changes:

1. For the low overpotential sulfur test, YSZ-Low, basically only $R_{Ni\text{-}TPB}$ is affected (reversibly) by H_2S poisoning. Significant irreversible increase in the high frequency part of the IS (ohmic resistance and ionic conductivity in the anode) was observed for the YSZ-Hi.
2. The results from the non-sulfur high overpotential (YSZ-no-S) test in this work and previously reported tests suggest that the irreversible long-term degradation for YSZ-Hi is closely linked to the sulfur addition.
3. The overpotential, rather than the current density or materials chemistry (since both YSZ and ScYSZ based anodes were tested), was found to be the key parameter for whether or not a given H2S-exposure led to long-term irreversible degradation of the Ni-Zirconia based SOFC anodes.
4. SEM shows that the cell from YSZ-Low and from the non-sulfur high overpotential (YSZ-no-S) test both have satisfying percolating Ni network and porosities as expected when compared with a non-long-term tested cell.

[3] A. Hauch, A. Hagen, J. Hjelm and T. Ramos, Journal of The Electrochemical Society, 161, F734 (2014).

5. SEM shows that the cell from YSZ-Hi has a significant lower phase fraction and number of percolating Ni particles in the few microns of the anode closest to the electrolyte. Furthermore, this anode has an increased phase fraction of porosity in this same region of the anode but similar number of pores when compared to other tested cells.

1.3.3.2.2 Nanostructured Anode Coatings This activity was comprised of two main tasks, the first of which was the screening of suitable materials for infiltration to enhance sulphur poisoning tolerance of the Ni-cermet electrode. This was carried out using miniature symmetrical cells. The infiltrates included Nb_2O_5 , Sc_2O_3 , CeO_2 , BCZYYb44 ($BaZr_{0.4}Ce_{0.4}Y_{0.1}Yb_{0.1}O_3$) and MgO at various loadings. Figure 12 shows a summary of the observed relative changes in polarization resistance as for reference anode samples and anode samples infiltrated with the different infiltrates.

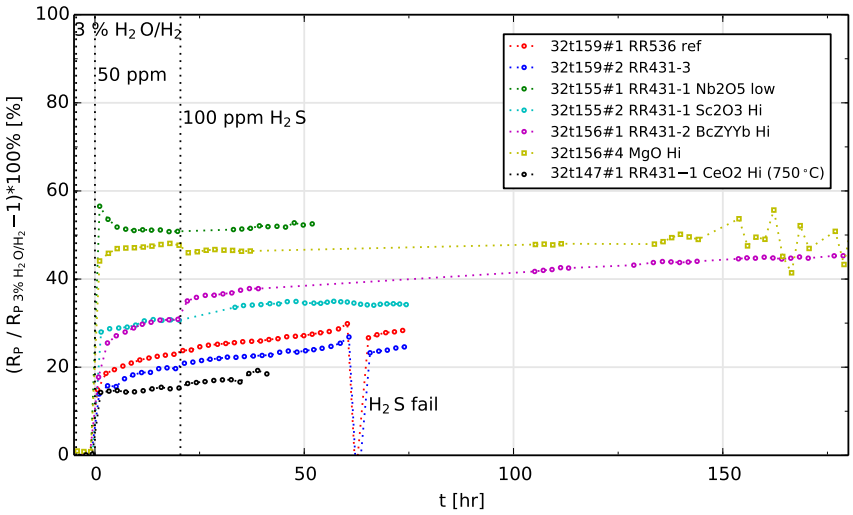

Figure 12: Time evolution of the normalized polarization resistance (R_p) at 700 °C for selected cells from three independent tests (a) 32t155 (Nb_2O_5 - lo, Sc_2O_3-hi), (b) 32t156 (BCZYYb44-hi, MgO-hi) and (c) 32t159 (reference, non-infiltrated) and d) 32t147 (CeO_2-hi) which in contrast to the other three tests was carried out at 750 °C. Where t = 0 correponds to the beginning of the H_2S feed (50 and 100 ppm).

The conclusions of the screening study were:

1. Most infiltrated cells exhibit a slightly higher R_p when compared to the references, but the level of difference for most could be easily explained by a higher contribution to gas diffusion from the infiltrated pores.
2. With the exception of CeO_2, all other tested infiltrates increased the initial degradation of R_p upon introduction of either 30 or 50 ppm of H_2S in 3% H_2O/H_2 compared to the reference, non-infiltrated cells. Increase of the H_2S concentration to 100 ppm only really further affects the BCZYYb cells.
3. CeO_2 infiltration shows some promise as a performance and tolerance enhancer.

The second activity was concerned with investigation of the preparation and testing of full cells that were reduced ex-situ (before they were placed in a cell test fixture), and the use of selected infiltrates from the screening study in the ex-situ reduced cells, a strategy which, if successful, would allow testing of infiltrates in single cells under relevant operating conditions and under current load. The need for pre-reduction arises from the low porosity (usually less than 12 %) of the as-sintered (oxidized) half-cells, which are not suitable for infiltration of additives into the active electrode area. After several trials, the developed pre-reduction protocol enabled acceptable cell flatness for testing. The half-cells were also deemed strong enough to undergo both cathode printing and testing. The final pre-reduction protocol for the concerned half-cells can be summarized as: (i) Ramp up in air from room temperature up to 1000 °C at a rate of 1 °C/min; (ii) Hold for 30 minutes in air at reduction temperature; (iii) Switch gas to moisturized 9% H_2 /N_2 reduction gas and hold for 1 hour; (iv) Cool down to room temperature at 1°C/min.

A series of half-cells (Ni-YSZ/YSZ) were reduced ex-situ using this protocol and subsequently dense CGO barrier layers were deposited using PVD on top of the electrolyte. As the cells were provided with a CGO barrier layer it was possible to use pure LSC as the cathode layer, which is an advantage as this

electrode is easy to fire in-situ and yields good results already at a temperature of 850 °C[4], which was also the maximum temperature and start-up temperature used in the single cell tests.

A number of tests were carried out with pre-reduced reference cells and a set of cells with CGO infiltrated into the pre-reduced porous anode. The tests with the pre-reduced reference cells (without infiltrate) were successful, with good leak tightness obtained and no cracks detected in the cells. However, all the tests with CGO infiltrated into the anode and anode support were of relatively poor leak tightness, indicating problems achieving a good seal with the sealant gasket used and/or cracks in the tested cells. Figure 13 shows leak test data collected during the initial phase of each test, and figure 14 shows polarization curves recorded at 850 °C for the tested cells. Consistent with the leak measurements the polarization curves of the infiltrated cells shows some signs of fuel starvation at high currents, most likely related to the observed leaks. It is not clear at the present why the testing success rate with the infiltrated cells is lower than with pre-reduced reference cells, and this problem was not solved within the project period. However, if successful, this may be a fruitful route to the study of anode coatings in the future.

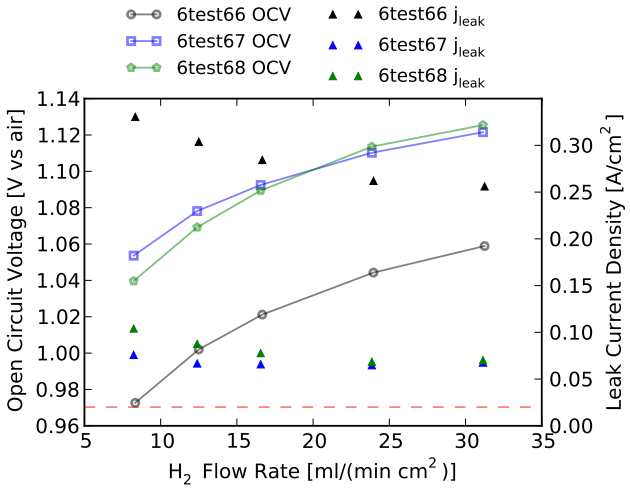

Figure 13: OCV values and calculated equivalent leak current density (based on an active area of 16 cm^2) as a function of fuel flow rate. The leak current is a quantitative measure of the total leak (external + internal) and does not represent an electronic leak through the cell. The dashed line illustrates the average leak current observed for the non-infiltrated cells.

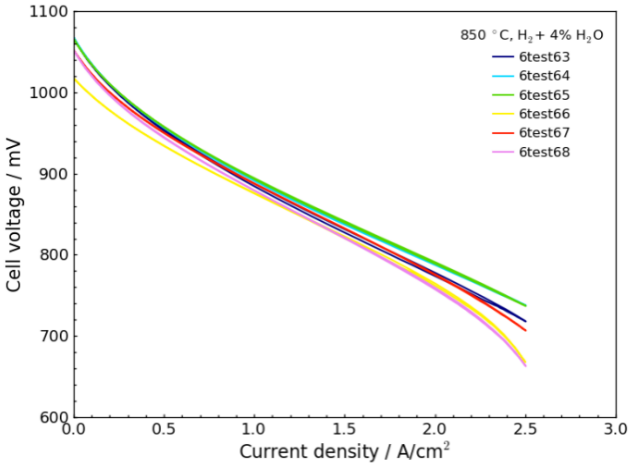

Figure 14: Polarization curves recorded of three pre-reduced cells without infiltrate (6test63-65) and for three cells with CGO infiltrated into the anode (6test66-68). The measurements were taken at 850 °C with a fuel flow of 25 l/h and a fuel composition of 4 % H_2O + 96 % H_2, and air as the oxidant.

1.3.3.3 WT3.2 – Detailed Characterization of Cells Operating in Reformate Gas A major goal of the project was to achieve an improved understanding of influence of reformate gas composition on the performance of cells operating under current. The origin and magnitude of various losses in the cell as well as information furthering the understanding of the parameter intervals of safe operation were to be determined. Furthermore, a detailed investigation of the additional performance-limiting low frequency process reported[5] for reformate mixtures was also targeted. These goals were addressed in WT3.2 and the corresponding milestone was M3.2 - "A comparison of the overvoltage - current characteristics of at least two different Ni-cermet anodes in reformate gas completed". Three different SOC types were investigated differing in (a) production procedure and (b) fuel electrode microstructure as summarized in Table 2. Cells A and B have a common half cell production method - multilayer tape casting and lamination (MTC) whereas cell C was produced using a combination of tape-casting and spraying. As a consequence of this difference cells A and B have a ~5 µm thick electrolyte and cell C a ~10µm thick electrolyte. Cell B however differs from cell A in that it has a finer (smaller particle size) anode structure. All cells had electrolytes coated with a thin CGO (1-2 µm) interdiffusion barrier layer deposited using a PVD technique.

[4] J. Nielsen, P. Hjalmarsson, M.H. Hansen, P. Blennow, "Effect of low temperature in-situ sintering on the impedance and the performance of intermediate temperature solid oxide fuel cell cathodes", *Journal of Power Sources*. 245 (2014) 418–428. doi:10.1016/j.jpowsour.2013.06.067.

[5] A. Kromp, A. Leonide, A. Weber, and E. Ivers-Tiffée, J. Electrochem. Soc., 158, B980 (2011).

Cell #	Cell-type	Anode-Support	Anode	Electrolyte	Barrier	Cathode	CCL
A	MTC	Ni-3YSZ	Ni-8YSZ	8YSZ (~5 µm)	CGO	LSC-CGO	LSC
B			Ni-8YSZ (finer microstructure)				
C	Non-MTC		Ni-8YSZ	8YSZ (~10 µm)			LSM

Table 2: Overview of tested Solid Oxide Cells

The characterization process entails providing the cell under test with selected fuel and oxidant compositions, stepwise increasing the current density, recording the impedance spectra and quantifying the individual area specific resistance (ASR) contributions through CNLS fitting using an appropriate equivalent circuit model (ECM). Integration of the ASRs with current density gives the overpotential related to the corresponding loss mechanism.

The cells were characterized at 700 °C in the current density range 0 - 0.5 A/cm^2 in three fuel gas mixtures H_2/H_2O, H_2/CO_2 and $CH_4/H_2/H_2O$ (0.8/0.2, 0.81/0.19, and 0.3/0.1/0.6 atm respectively) as summarized in Table 3. The operation points were chosen such that the fuel utilization at the highest current density (0.5 A/cm^2) was 60% at the fuel electrode and 20% at the oxygen electrode. Table 3 also displays the theoretically expected equilibrium concentrations in the reformate mixtures.

Gas (atm)	Inlet composition (mole fractions)				OCV (mV)	FU at 0.5 A/cm^2 (%)	T (°C)
	H_2/H_20	Reformates					
		Ref. 1	Ref. 2	Equilibrium composition			
H_2	0.8	0.81	0.1	0.64	1030	60	700
H_2O	0.2	-	0.6	0.16			
CO_2	-	0.19	-	0.05			
CO	-	-	-	0.13			
CH_4	-	-	0.3	0.02			

Table 3: Inlet gas compositions

The recorded impedance spectra were then fit with an ECM consisting of a series resistance (R_s) for the ohmic losses, two RQ-elements for the fuel electrode electrochemical processes (coupled gas diffusion, charge transfer and ionic conductivity in the anode functional layer, AFL)[6], a Gerischer element for the oxygen electrode electrochemistry (surface exchange kinetics and O^{2-} ion bulk diffusion)[6], a Warburg element for diffusion in the substrate, an RQ element for gas conversion[7] ASR and for spectra recorded in reformate mixtures RQ element for extra process at the lowest frequency[5]. This ECM is displayed in figure 15.

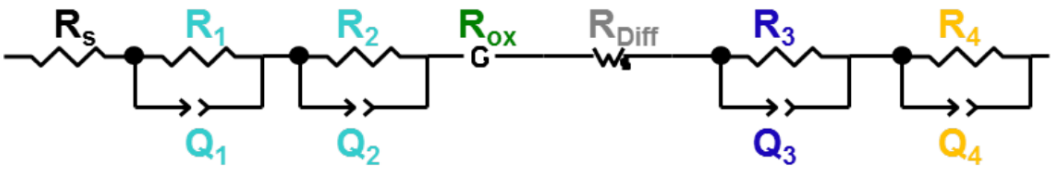

Figure 15: Equivalent Circuit Model (ECM) used for CNLS fits.

The CNLS fit of the recorded spectra with the ECM in figure 15 entailed a pre-identification of the processes using the method of re-calculation of the impedance data into a distribution of relaxation times (DRT)[8] for the initial values. To this end, spectra recorded at 0.5 A/cm^2 were used for the starting values (better resolution of individual peaks) and then at decreasing currents down to OCV.

[6] A. Leonide, V. Sonn, A. Weber, and E. Ivers-Tiffée, J. Electrochem. Soc., 155, B36 (2008).
[7] S. Primdahl, M. Mogensen, in 5th International Symposium on Solid Oxide Fuel Cells, (1997).
[8] H. Schichlein *et al*, J. Appl. Electrochem., 32, 875 – 882 (2002)

1.3.3.3.1 DRT analysis of EIS under load Figure 16 displays the DRTs of the EIS spectra recorded under current load at the investigated three gas mixtures for the three cells. Due to a technical fault useful data in the CH_4 containing reformate mixture could not be recorded for cell A. This however is not critical to the objective of the project which was aimed at carrying out these investigations in at least two different cell types. The processes can be grouped into three frequency regions:

1. *Fuel electrode electrochemical reactions (f > 1 kHz)*
   The performance of the three cells differs slightly with cell B (finer anode structure) showing the best performance in all gas mixtures, followed by cell A and then cell C. However, cells B and C display comparable performance in both reformate mixtures and a slightly better performance in the H_2/H_2O mixture.
2. *Oxygen electrode and substrate (anode-support) diffusion (10 < f < 1kHz)*
   The ASR of the LSC/CGO oxygen electrode is very small and to an extent overlaps with the substrate diffusion ASR. Comparable behavior can be observed for all three cells in all fuels despite a slightly larger and less "scatter" in cell A.
3. *Gas conversion and reformate processes (f < 30 Hz)*
   In H_2/H_2O fuel, all three cells display a single peak with comparable ASR. In reformate mixtures, again all three cells display comparable behavior in that they all show two peaks with same behavior under current load. However, cells A and B seem a bit more comparable to each other than to cell C, especially in the H_2 /CO_2 mixture.

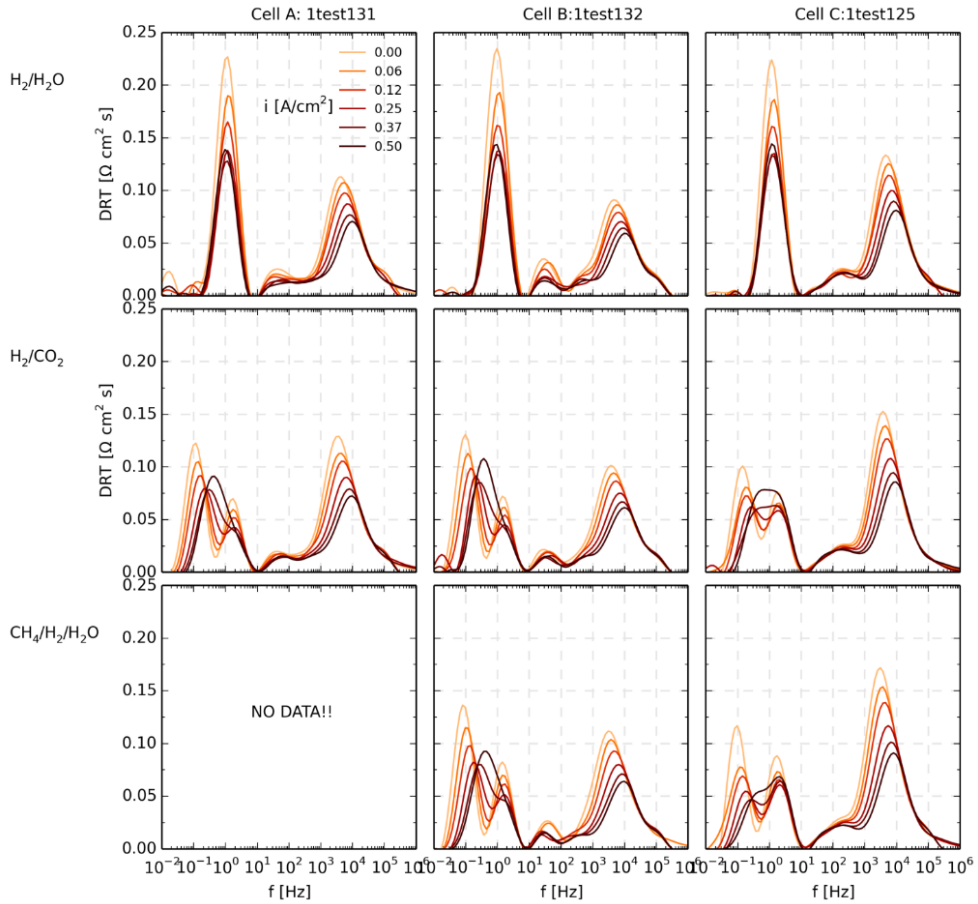

Figure 16: DRT plots of cells A, B and C re-calculated from EIS spectra recorded at 700 °C in the fuel mixtures H_2/H_2O, H_2/CO_2 and $CH_4/H_2/H_2O$ (0.8/0.2, 0.81/0.19, and 0.3/0.1/0.6 atm, respectively) at varying current density from 0 - 0.5 A/cm^2 in (0 - 60% fuel utilization).

1.3.3.3.2 Overpotential vs Current Density Relations From the qualitative analysis above it is evident that except for the distinguishably better performance of the fuel electrode of cell B (the cell with a finer anode) cells A and B are quite similar. This coupled with the lack of data for CH_4 reformate mixture for cell A, makes it more reasonable to do a quantitative comparison on cells B and C alone – two SOCs differing in production method as well as fuel electrode microstructure. The overpotential *vs* current density plots for cells B and C are displayed in figure 17. Comparing both cells in the three fuel mixtures at a current density of 0.3 A/cm^2 for instance confirms the following significant differences:

- The finer Ni-8YSZ cermet fuel electrode of cell B is yielding a significantly smaller overpotential contribution than that of cell C.
- The ohmic contribution of cell C to the total voltage drop is twice as large as that of cell B, due to the twice as thick electrolyte in cell C.
- The contribution from the low frequency reforming process is slightly larger for cell B than cell C.
- The oxygen electrode of cell C is yielding a slightly larger overpotential contribution that that of cell B.

This work corresponds to fulfilment of Milestone 3.1 - "A comparison of the overvoltage – current characteristics of at least two different Ni-cermet anodes in reformate gas completed".

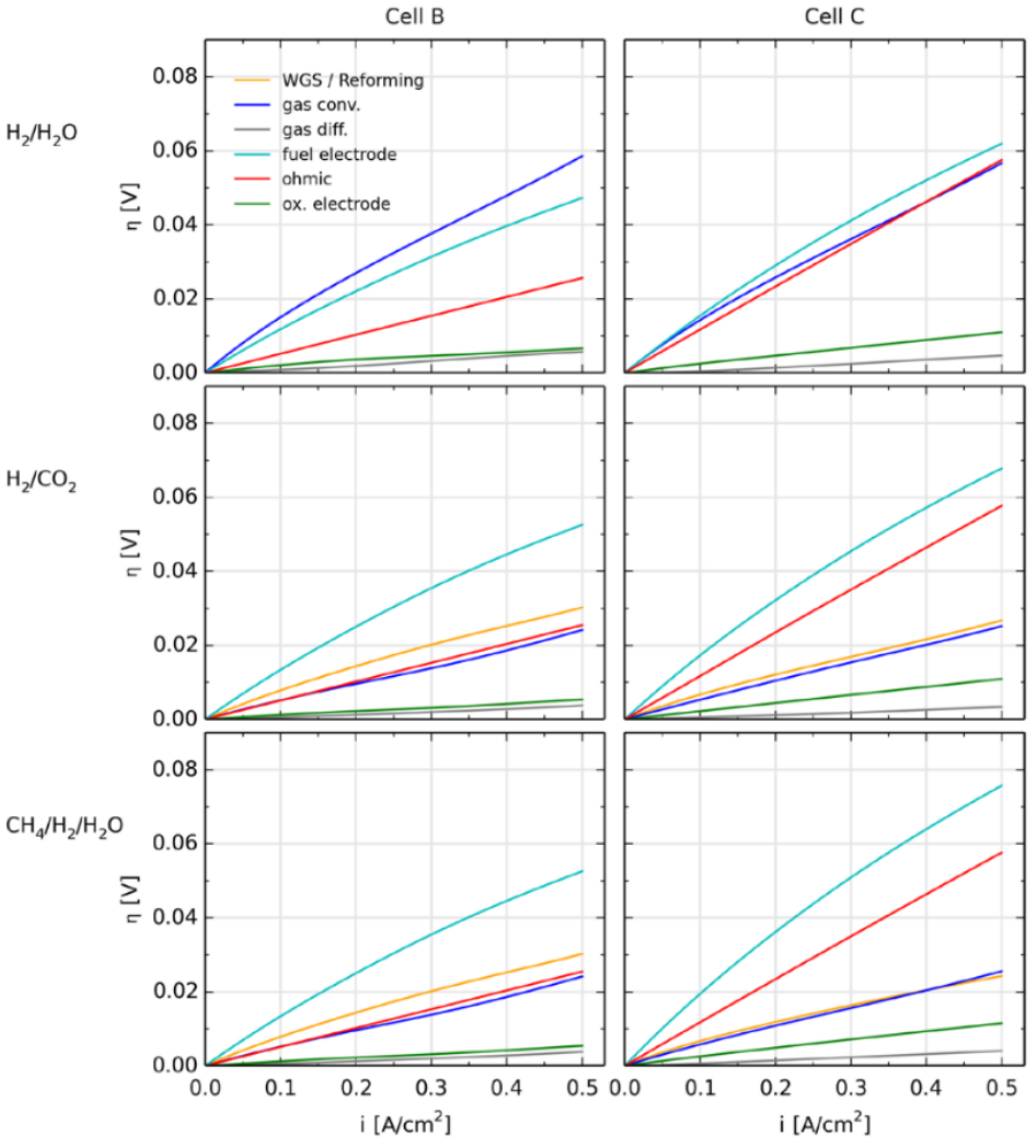

Figure 17: Overpotential *vs* Current density relations of cell B vs C at 700 °C in the fuel mixtures H_2/H_2O, H_2/CO_2 and $CH_4/H_2/H_2O$ (0.8/0.2, 0.81/0.19, and 0.3/0.1/0.6 atm, respectively) obtained by integration of the process specific differential resistances quantified by CNLS fitting of the used ECM (figure 15) to the collected impedance data.

1.3.3.4 WT3.3 - Durability at Constant Load in Reformate Gas Together with WP1 and WP4 a few key test gas compositions were identified that could be used for durability testing in the project. One of these gas compositions closely corresponds to that suggested for the standardized test module "TM 06-HD internally steam reformed (ISR) methane pre-reformed at 10%; Heavy Duty Test module" in the EU-JRC report "SOFC Single Cell Performance and Endurance Test Modules"[9] following on from the work carried out under the FCTESTNet and FCTESqa projects. The suggested gas composition

[9] "SOFC Single Cell Performance and Endurance Test Modules", Test Modules TM SOFC 01-04LD / 05-08HD, 2010

corresponds to an OCV of 1.032 V vs air, but is diluted with 50% nitrogen. Nitrogen was omitted from the gas mixture used for stability tests in this project.

The half-cell was produced by tape-casting and lamination, and the tested cells correspond to cell A in table 2 In order to investigate the stability of the cells during the initial ~1000 h of operation, tests were carried out in three different gas compositions:

- *H_2/H_20 fuel*:
  corresponding to the "TM 05-HD - Heavy Duty Test Module with Hydrogen", i.e. H_2/H_2O = 0.6/0.4 (OCV = 0.990 V vs air at equilibrium at 700 °C) operated at flows yielding a fuel utilization of 20%.
- *Internally steam reformed methane (ISR-CH_4):*
  as suggested for TM 06-HD ($CH_4/H_2O/H_2$ = 0.3/0.6/0.1, OCV = 1.031 V vs air at equilibrium at 700 °C) but without dilution with N_2operated at conditions yielding a fuel utilization of ~ 60%.
- *"Externally reformed methane (ESR-CH_4)"*:
  in a custom gas mixture containing CO and CO_2 ($H_2/H_2O/CO/CO_2$ = 0.64/0.09/0.04/0.23, OCV = 1.007 V vs air at equilibrium at 700 °C) operated at conditions yielding a fuel utilization of ~ 60%. The suggested composition for ESR-CH_4 in module TM 07-HD (see footnote 9) is slighty different ($H_2/H_2O/CO/CO_2$ = 0.72/0.06/0.00/0.22, OCV = 1.013 V vs air at equilibrium at 700 °C) to the composition used here.

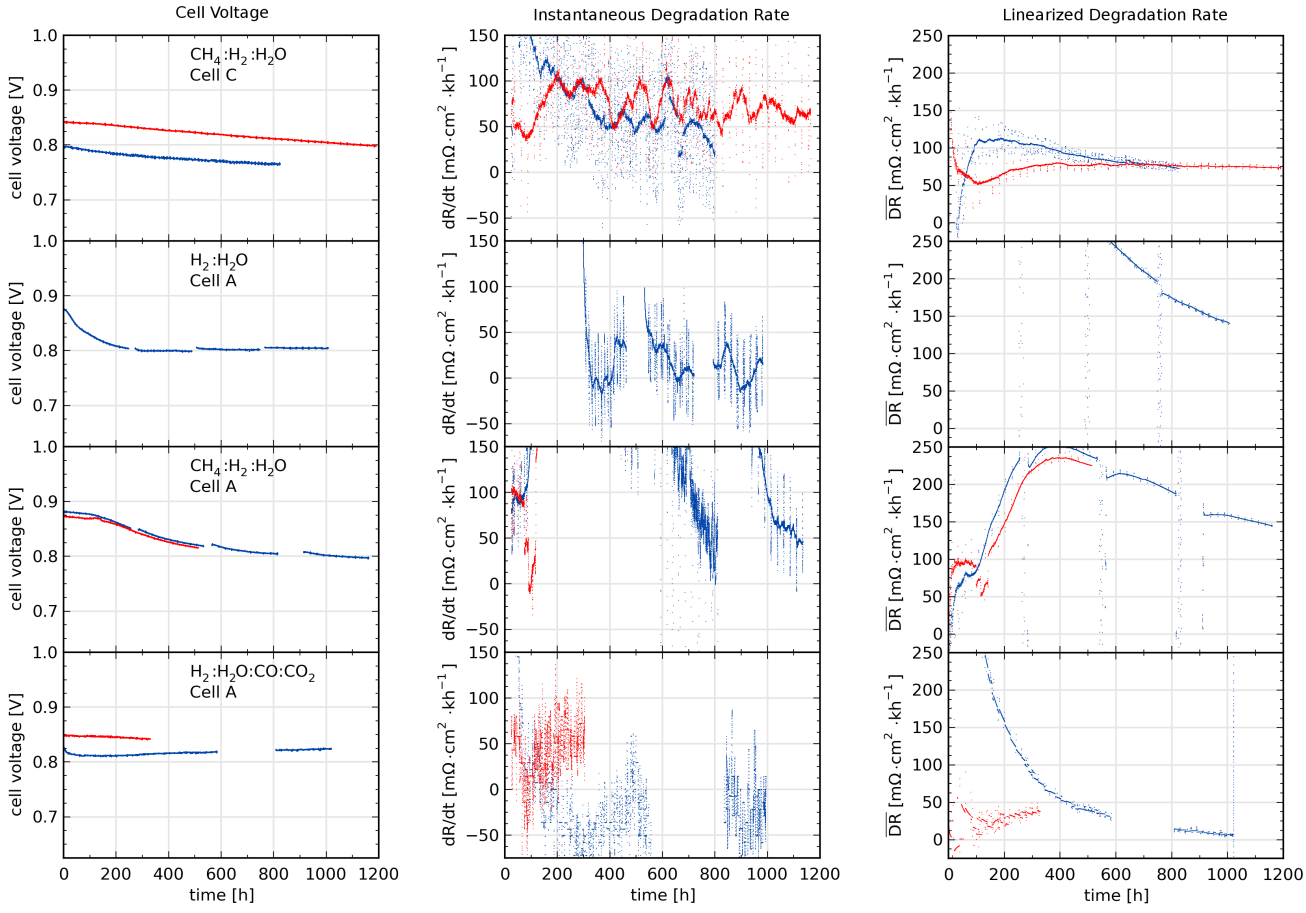

Figure 18: Galvanostatic durability tests carried out at 700 °C and a current density of 0.5 A cm^{-2}. The four plots in the middle column shows the instantaneous degradation rate (dR/dt) as a function of time. The periodic part of the "noise" in the data is caused by voltage oscillations caused by impedance measurements. The plots in the right column shows the linearized degradation rate, i.e. the total degradation at each time re-calculated to a degradation rate. If one observes linear degradation the $\frac{dR}{dt}$ and $\overline{DR}$ yield the same value, exemplified by thee second test of Cell C - red markers/lines in the top row of graphs. The calculation of both degradation rates assumes a constant OCV thoughout the test. For tests with varying degradation rate, the instantaneous degradation rate observed at long times is a better measure of the long term degradation rate. The missing cell voltage data for the first test in H_2:H_2O:CO:CO_2("ESR-CH_4") was due to data logging problems, but the test was running for the whole period (blue curves on the fourth row of plots).

The first durability tests using cells corresponding to cell C in table 2 were carried out using methane reformate fuel gas (ISR-CH_4). A further five durability tests were started during the project, three of which are completed by the end of the project. The last two tests are repeat tests to investigate the reproducibility of the durability data. The cell voltage history plots, the instantaneous degradation rate (dR/dt), and the linearized degradation rate,[10] as a function of operating time in seven durability tests carried out, mainly using cells corresponding to Cell A in table 2, are displayed in figure 18.

The test in H_2/H_2O and the first test of Cell A in ISR-CH_4($CH_4/H_2O/H_2$) was interrupted every ~250 h for a full characterization of the cell at 700 °C, which was also the durability test temperature. The cell activated slightly after the characterization period, and this complicates the DC degradation analysis somewhat. During the characterization the cell was held at OCV for most of the time (to allow impedance data to be recorded at OCV), and multiple polarization curves were also recorded with a lower cut-off voltage of 0.6 V (to avoid re-oxidation of the anode). As expected from the previously reported work of A. Hauch et al[11] and others, the performance of the cell tested in H_2/H_2O decreases rapidly in the beginning of the test (during the first ~ 50 - 200 h depending on the water content in the fuel gas, at 750 °C), most likely due to coarsening of the Ni-phase in Ni-YSZ cermet anode, and possibly also due to impurity segregation to the Ni-YSZ-pore triple-phase-boundary (TPB). The initial degradation in the tests with $CH_4/H_2O/H_2$ was significantly slower, but interestingly, the completed first test indicates that the performance stabilizes at nearly the same cell voltage (0.8 V) as in the H_2/H_2O test. The two tests in the "ESR-CH_4" mixture displays differences in the stability, and further testing would be necessary to establish the influence of these conditions on the stability fully. In general, the initial degradation observed in the tests of Cell A (mainly anode degradation) is slower in ISR-CH_4 than in H_2/H_2O, and appears even slower, or of smaller magnitude, in "ESR-CH_4". The results obtained so far gives an overview of the degradation of two types of cells (differing mainly in the anode) over the initial 1000 h. Cell A (an improved cell produced in WP6 in this project) yields a very stable cell voltage after approximately 250 h in H_2/H_2O, but needs to be repeated without interruptions during the test.

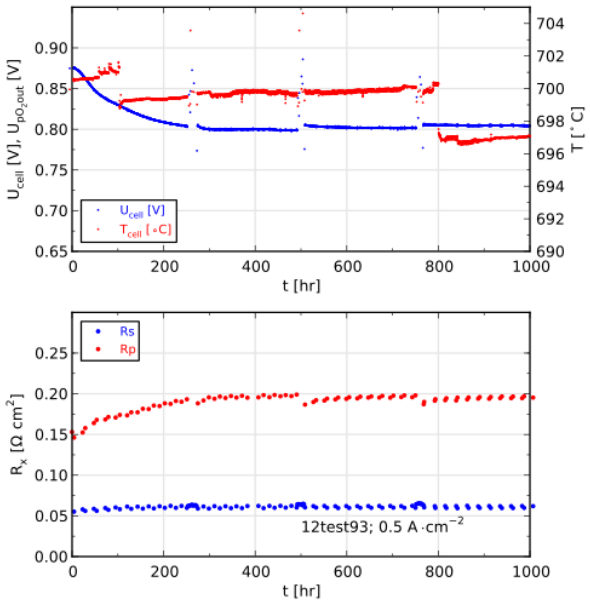

Figure 19: Uppper graph: Cell voltage and measured cell temperature throughout the H_2/H_2O durability test. Lower graph: Evolution of the series (R_s) and the polarization resistance (R_p).

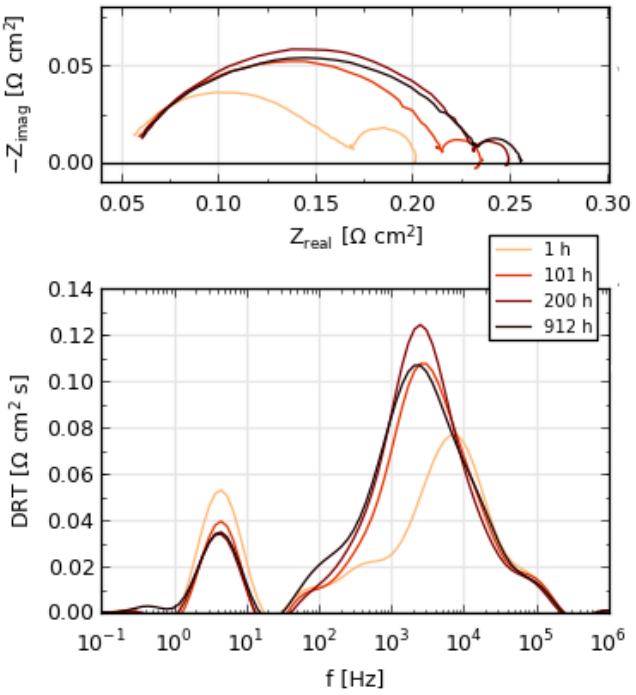

Figure 20: DRT analysis of selected impedance spectra collected at different times during operation. The large increase in the frequency range 1 - 10 kHz corresponds to changes in the anode polarization. The slight decrease of the impedance in the frequency range 1-10 Hz corresponds to the gas conversion resistance.

The evolution of the polarization resistance (R_p) and the ohmic resistance (R_s) of the cell tested in H_2/H_2O is illustrated in figure 19. A DRT analysis of the impedance recorded at selected times during

[10] R.S. Gemmen, M.C. Williams, K. Gerdes, Degradation measurement and analysis for cells and stacks, Journal of Power Sources. 184 (2008) 251–259. doi:10.1016/j.jpowsour.2008.06.047.

[11] A. Hauch, M. Mogensen, A. Hagen, Ni/YSZ electrode degradation studied by impedance spectroscopy - Effect of p(H_2O), Solid State Ionics. 192 (2011) 547–551. doi:10.1016/j.ssi.2010.01.004.

the test is shown in figure 20 and confirms that the anode displays the largest resistance change during the test. The degradation of two different cell types in reformate gas was studied in the project and corresponds to a (partial) fulfilment of milestone 3.2, but further work is necessary, including longer tests, and a bigger data set (more replicate tests), to establish accurate long-term degradation rates in carbonaceous fuels. The obtained results raises questions about the influence of idling, degree of polarization, and transient operation on the cell stability which may be further explored in the project SOFC4RET [ForskEL project no. 2014-1-12231].

1.3.3.5 Porous Electrode Theory applied to Solid Oxide Cell Electrodes The interpretation of electrochemical impedance spectra in terms of equivalent circuit models is a central tool in the evaluation of solid oxide single cells and symmetrical cells. A detailed study of the electrochemistry of the composite LSM-YSZ electrode (a common SOFC cathode) and review of the use of porous electrode theory was started in the previous project (ForskEL 2010-1-10441) and completed in this project. It was shown through a comprehensive impedance spectroscopy study that the impedance of the classic composite LSM-YSZ (lanthanum strontium manganite and yttria stabilized zirconia) SOFC cathode can be described well using porous electrode theory. Furthermore, it was illustrated through a literature review on SOFC electrodes that porous electrode theory not only describes the classic LSM-YSZ SOFC cathode well, but porous SOFC electrodes in general (figure 21).

The extensive impedance spectroscopy study of LSM-YSZ cathodes consisted of measurements on cathodes with three different sintering temperatures and hence different microstructures and varying degrees of LSM/YSZ solid state interactions. LSM based composite cathodes, where YSZ was replaced with CGO was also studied in order to acquire further knowledge on the chemical compatibility between LSM and YSZ. All impedance measurements were acquired in the very broad temperature range of 200–900 ◦ C for complete elucidation of the impedance. All impedance spectra were analyzed in terms of porous electrode theory (involving transmission line circuits). Physical materials parameters were extracted from the analysis, which were in excellent accordance with literature values. Valuable insight about the dissolution of Mn in the cathode composite material YSZ during preparation was furthermore provided along with valuable engineering characteristics such as the electrochemical utilization thickness. Further details can be found in the publication on this topic.[12]

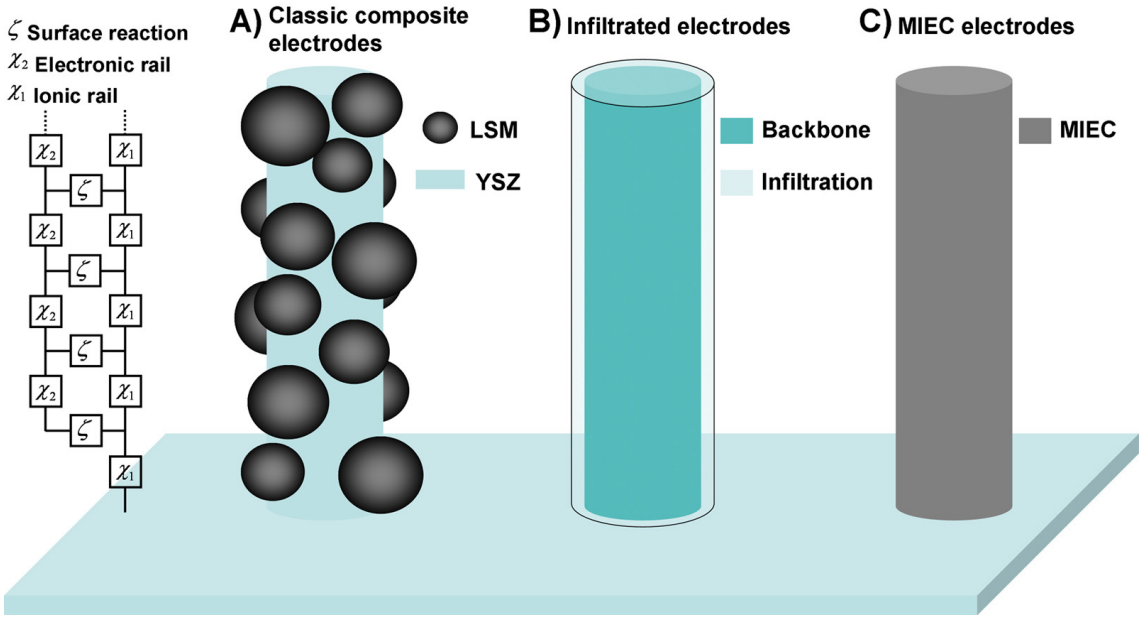

Figure 21: Transmission line describing the various SOFC electrode models. (A) Model of classic composite electrodes. In this particular case the LSM:YSZ composite cathode. (B) Model of an infiltrated electrode. (C) Model of a mixed ionic electronic conductor (MIEC) material based cathode.

A detailed analysis of the performance of Ni-ScYSZ cermet electrodes using porous electrode theory was also completed in this project.[13] The combined use of CNLS and DRT for impedance data analysis allowed an easier, less subjective, comprehensive study of Ni-ScYSZ electrodes under various operating conditions, cell designs, electrode thicknesses, as well as upon low temperature redox cycling.

[12] J. Nielsen, J. Hjelm, Impedance of SOFC electrodes: A review and a comprehensive case study on the impedance of LSM:YSZ cathodes, Electrochimica Acta. 115 (2014) 31–45. doi:10.1016/j.electacta.2013.10.053.

[13] T. Ramos, M. Søgaard, M.B. Mogensen, Electrochemical Characterization of Ni/ScYSZ Electrodes as SOFC Anodes, J. Electrochem. Soc. 161 (2014) F434–F444. doi:10.1149/2.045404jes.

From this study it was possible to confirm the existence of three main contributions limiting the performance of the electrodes. Applying a transmission line model (porous electrode theory) to describe the electrochemical processes, as well as generalized finite length Warburg (GFW) impedances for gas transport related processes, the associated resistances have been quantified. The results were found also in good agreement with the qualitative analysis provided by DRT. The resulting values were then normalized to suitable microstructural parameters. Both the extracted values of the ionic conductivity and the line specific charge transfer resistance were in very good agreement with what has been reported in the literature.

The presence of the anode support increases the resistance related to the gas diffusion, and one could tentatively conclude that it is not beneficial to have an anode support layer, even though the resistance associated with the electrochemistry decreases. However, the diffusion resistance in the low X_{H_2O} range scales with $X_{H_2O}^{-1}$, the resistance associated with the charge transfer process scales with approximately $X_{H_2O}^{-0.5}$ and the overall resistance of the anode transmission line model (TML) only with $X_{H_2O}^{-0.32}$. Therefore, at higher steam contents the resistance associated with the presence of the support layer becomes significantly smaller than the resistance associated with the combined ionic transport/charge transfer processes occurring at the Ni-ScYSZ cermet. Figure 22 illustrates the anode transmission line model in conjunction with the GFW's used to model diffusion through the support and a stagnant layer.

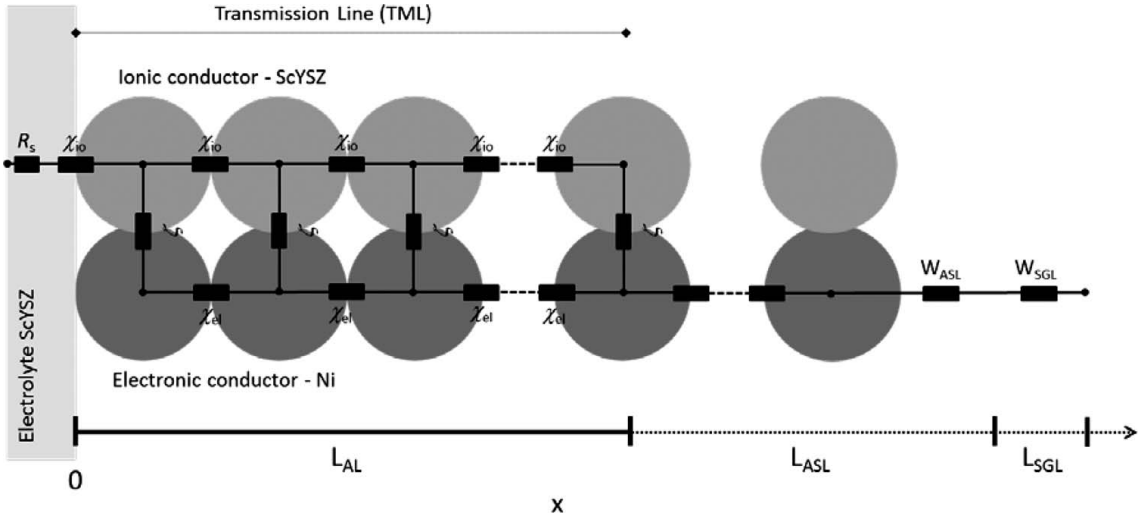

Figure 22: Illustration of the complete equivalent circuit combining TML and GFW impedances for anode-supported cells. For electrolyte supported cells, the absence of the anode support layer (ASL) eliminates $L_{ASL}$and W_{ASL} from the circuit.

1.3.3.6 Refinement of the Analysis of Impedance Data Low internal resistance and long-term stable performance are the two main properties needed for development of commercially attractive SOFCs. It is therefore of great importance to be able to quantify in detail the resistances of the individual components of the cell and how these resistances change over time, in order to design better cells and/or adjust operating conditions.

Impedance spectroscopy is a powerful technique for detailed study of the electrochemical and transport processes that take place in SOFCs, and impedance measurements contain all of the desired information. Meaningful analysis of impedance data is nontrivial, however, because a large number of modeling parameters are fit to the many processes which often overlap in the same frequency ranges. Also, commonly used equivalent circuit (EC) models only provide zero-dimensional (0-D) approximations of the processes of the two electrodes, electrolyte and gas transport. Employing improved analytical techniques to provide good guesses for the modeling parameters, like transforming the impedance data to the distribution of relaxation times (DRT), together with experimental parameter sensitivity studies, is the state-of-the-art approach to achieve good EC model fits. Here we present new impedance modeling methods which advantageously minimize the number of modeling parameters and the parameters used have direct physicochemical meaning.

1.3.3.6.1 Visualization First, we have refined our advanced visualization techniques used to identify the different electrochemical and transport processes that contribute to the impedance (Fig. 23). The DRT (Fig. 23d) and the difference in DRT spectra (Fig. 23e) clearly show that there are 5 impedance

processes that are affected by changes in either fuel or oxidant gas composition. Considering also the temperature dependence of these processes (not shown), they can be ascribed as follows (labeled in Fig. 23e):

1. $P_{1,FC}$ is fuel gas conversion
2. $P_{2,OD}$ is oxidant gas diffusion
3. $P_{3,FD}$ is fuel gas diffusion
4. $P_{4,OP}$ is oxygen-electrode polarization
5. $P_{5,FP}$ is fuel-electrode polarization

This progress in visualization is important because clear visualization is a critical part of developing an appropriate model and providing reasonable estimates of the parameter values to the model.

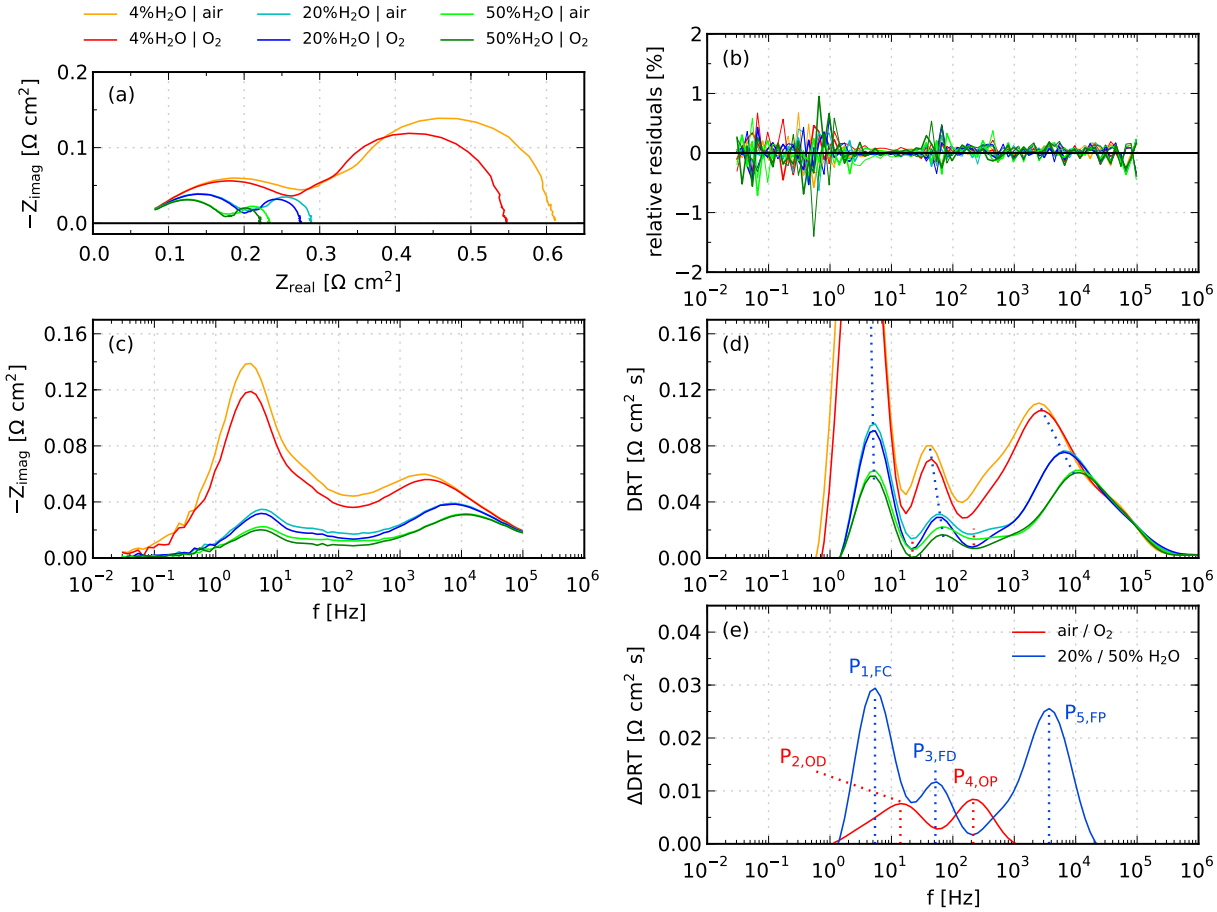

Figure 23: Visualization of 6 impedance spectra measured at 750 °C on one of the state-of-the-art Ni-YSZ | YSZ | CGO | LSC-CGO cells produced in our lab. (a,c) Raw cell data with only inductance removal applied; (b) Relative residuals of the linearized Kramers-Kronig test, illustrating high data quality; (d) The impedance transformed to the DRT; (e) The difference in DRT for changes only of the oxidant gas and fuel gas, which clearly shows the five individual impedance processes. The fuel composition was H_2 + the indicated amount of water, and air or oxygen as the oxidant, as indicated.

1.3.3.6.2 Modeling In the prior ForskEL "Durable and Robust SOFC" project, we made considerable progress in implementing an improved cell impedance model where the representative 0-D resistive-capacitive type EC "RQ" elements[14] are replaced by analytical 1-D porous electrode (PE) and 1-D or 2-D gas transport models. The gas transport models include 1-D gas diffusion (GD) through a porous layer or stagnant gas layer, 1-D plug-flow gas conversion (GC) along the flow channel, and 2-D coupled gas

[14] R. Barfod, M. Mogensen, T. Klemenso, A. Hagen, Y.-L. Liu, P.V. Hendriksen, J. Electrochem. Soc. 154 (2007) B371.

diffusion and conversion (GCD).[15] The improved model has fewer unknown parameters for the same number of processes, which advantageously decreases the total number of modeling parameters, and the parameters have direct physicochemical meaning (for example, microstructural parameters like porosity and tortuosity) which yields more detailed direct information about the cell processes. See also section 1.3.3.5 about porous electrode modeling.

Now we have further developed that model and we have developed a new model fitting algorithm, "multi-fitting", in which multiple impedance spectra are fit simultaneously with parameters linked based on the variation of measurement conditions, which greatly minimizes the total number of modeling parameters as well as subjectivity during modeling, thereby improving modeling accuracy. Using these methods, the number of fitting parameters for four impedance spectra measured with isolated changes to the fuel and oxidant gas compositions, has been *reduced from 80 to 25-34 depending on the model*. The methods have been implemented in our in-house data analysis software package mentioned in the prior "Durable and Robust SOFC" final project report (ForskEL 2010-1-10441).

The results of using the new model with multi-fitting are compared with the old model in Fig 24, using the same data shown in Fig 23. The old 0-D model (Fig 24a) fits the data similarly well as the new model with coupled gas transport (Fig 24c) as well as a new intermediate model with individual GD and GC sub-models (Fig 24b). However, the resistance values vary by as much as 30%, differences which can be very important e.g. when determining overpotentials (see section 1.3.3.3.2) of cell components.

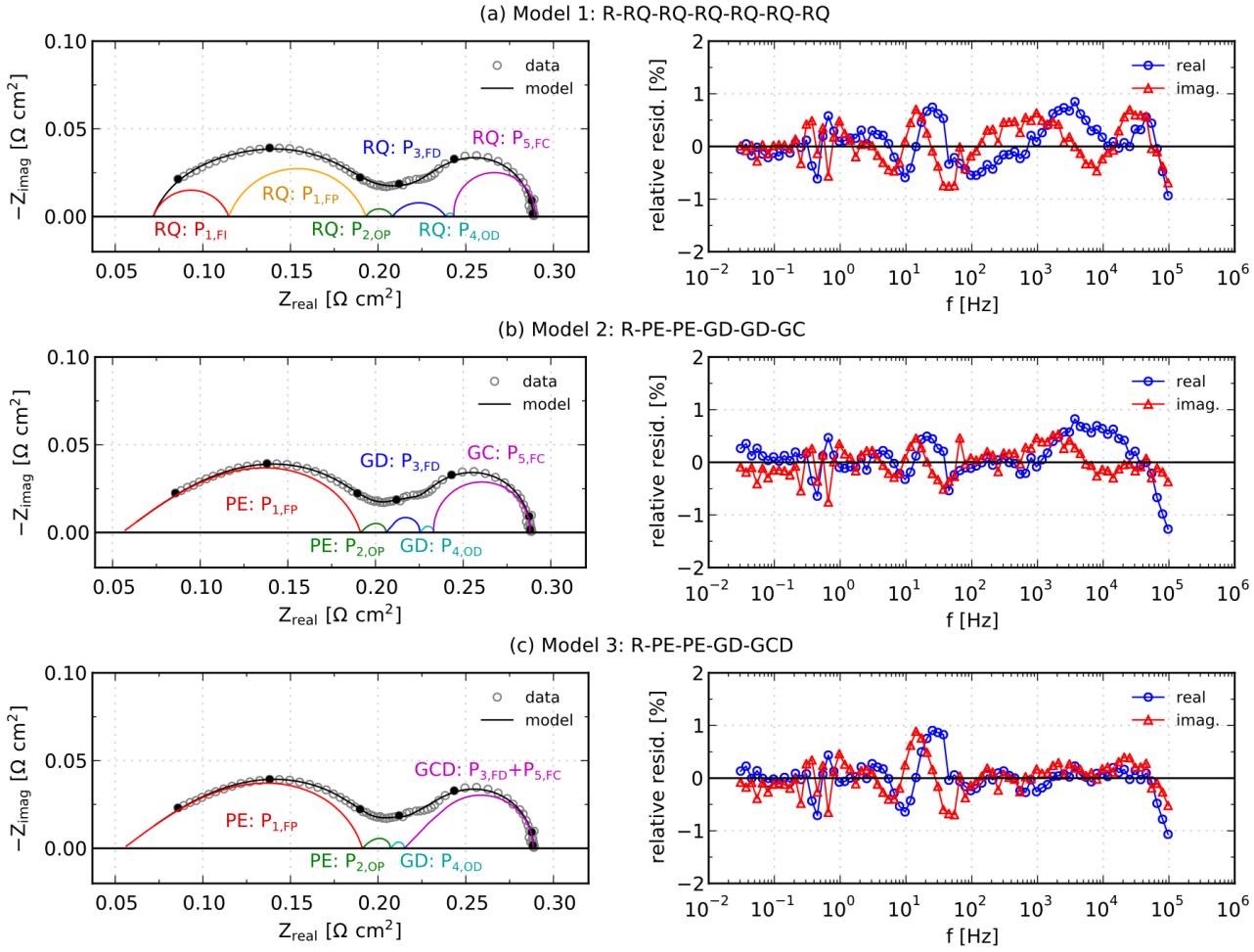

Figure 24: Model fitting results for an impedance measurement at 750 °C, 20% H_2O (balance H_2) supplied to the fuel-side and air to the oxidant-side, for (a) Model 1, (b) Model 2, and (c) Model 3.

The improved accuracy of the new model with multi-fitting is illustrated in Fig 25a, which shows improved results obtained for parameter variations such as the PE model parameters. Shown are the single-fitting vs multi-fitting results of the parameters ionic conductivity σ_{FI} and electrochemical reaction resistance r_{FP} for the fuel-electrode polarization process $P_{5,FP}$, as well as the oxygen-electrode polarization resistance R_{OP}. The same settings were used during the two different types of fitting. Multi-fitting clearly captures a log-log trend for r_{FP} vs pH_2O, unlike single-fitting. Even more striking are the results for R_{OP}, which should not have any dependency on pH_2O on the other side of the cell.

[15] T. Jacobsen, P.V. Hendriksen, S. Koch, Electrochimica Acta 53 (2008) 7500.

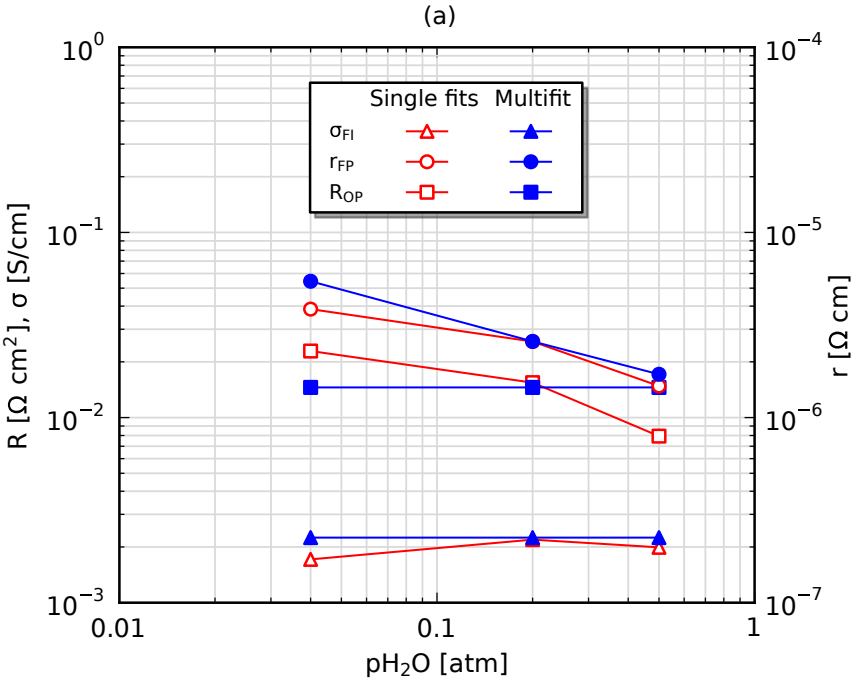

Figure 25: Comparison of single-fit and multi-fit results vs pH_2O for (a) $P_{5,FP}$ and $P_{4,OP}$ parameters using a PE model in Model 2 and 3, and (b) $P_{3,FD}$ resistance using RQ element in Model 1.

With the single-fit results, there is a significant and incorrect dependency which is due to interference during fitting from overlapping impedance processes that do have pH_2O dependency. The overlapping processes have much larger impedance than that of the very high performance LSC-CGO oxygen-electrode, which comprises only ~5% or less of the total impedance and is therefore very challenging to analyze (but also valuable to quantify e.g. for determining long-term stability of the electrode). In multi-fitting, on the other hand, the parameter has no pH_2O dependency because it has been defined as independent of pH_2O by linking it as a single parameter for all 3 spectra which have differing pH_2O. Multi-fitting converges the R_{OP} to the value that best fits all of the 4 spectra used in the multi-fit.

Another example that illustrates the advantage of multi-fitting is the polarization resistance of the fuel side gas diffusion process $P_{3,FD}$, again with the pH_2O variation (Figure 25b). In this case the theoretical trend of the diffusion resistance with pH_2O is well known.[16] In this example the gas diffusion process was fit to an RQ element. Fitting it to a GD model would force the theoretical expected pH_2O dependency. Instead, the intention was to see how well the dependency could be captured. The multi-fit results clearly capture the expected trend much better than the single-fit results. Further detail about these advanced impedance modeling methods are described in our recently published proceeding article.[17]

1.3.4 WP4 - Stack Mapping & Testing

This work package is where all characterization of stacks was carried out. The overall purpose of WP4 was to test the stacks using conditions defined in WP1 and to carry out mapping of 1) electrical efficiency 2) occurrence of hard failures, and 3) local properties in a stack such as temperature distribution, contacting, and fuel flow distribution. This activity was headed by TOFC and the work carried out by TOFC and DTU Energy Conversion (Risø).

1.3.4.1 WT4.1 & WT4.2 – Testing and Mapping of Operational Modes at Constant Load and under Dynamic Operating Conditions In WP1 a number of operating modes were defined ("idle", "nominal load", and "power burst/max load") out of which operation at nominal load is the most important, and these suggestions were used to evaluate different key operational modes for stacks operated at constant load. Figure 26 shows data from an extended multiple load cycle and idle operation test of

[16] S. Primdahl, M. Mogensen, J. Electrochem. Soc. 146 (1999) 2827

[17] C. Graves, J. Hjelm, "Advanced impedance modeling of solid oxide electrochemical cells ", Proc Eur. Fuel Cell Forum 2014, B1203

a stack. This test covers 19.8 hours at H_2 OCV operation, accumulated >34 hours at OCV in NG/CPO[18] fuel and finally a 13.8 hour period at OCV in CPO operation. No performance issues were observed.

The main concern for the stack operation at low FU in partially reformed NG is the thermal impact where internal reforming cooling at the inlet side of the stack is unbalanced by reaction heating and ASR heating from operating the stack at load. The OCV condition is therefore to be considered a thermally worse operating condition than operating at a load.

The NG operation at OCV in the case illustrated by figure 26 was performed as 45 min cycles. For each cycle the OCV stabilizes to very near its maximum value, which shows that near thermal equilibrium for the maximum internal reforming cooling is reached within this time as well. The fact that the test is operated in a cyclic manner is considered a harder test than for constant OCV over prolonged time.

Data from more than ten stacks were used for evaluation of the different operating modes, and the table below summarizes the tests and how they relate to the suggestions from WP1. Apart from the above extended test, the tested stacks have also seen 5 such OCV cycles, confirming stability over a larger number of stacks.

The stack tests data documented above cover the main part of the suggested goals from WP1. Conditions that are not covered are:

1. Up to 0.5 A/cm^2 current density was suggested but up to 0.42 A/cm^2 has been tested. The higher current density operating points were performed in CPO operation. For the higher current densities running in CPO operation may be considered more challenging as the total fuel flow is considerably higher for CPO operation than for NG operation and thus set a higher demand for proper fuel distribution.
2. Transient up has been shown to be fast enough but has not been tested directly from lower than 25% of maximum power and up. Here the lower target was 10%. In the conducted load cycles, increased load is performed as abrupt steps from 0A to 10A then to 25A/40A after 45 minutes stabilization at 10A. There is no specific reason to believe that going directly from 0A to 25A/40A should introduce issues not observed in the present test.
3. Start-up times of down to 30 minutes were suggested but due to limitation of the test rig heating capabilities, no faster than 90 minutes have been realized in these tests.

Overall the stack tests documented above show that the stacks are quite capable of meeting the majority of the demands suggested for smart grid evaluation. None of the identified demands have been shown to cause problems for the stacks but some have not been fully tested as mentioned above.

An aspect that must be considered for future work is the verification of similar performance capability for aged stacks that have run for periods close to the end of the specified lifetime of the given stack generation.

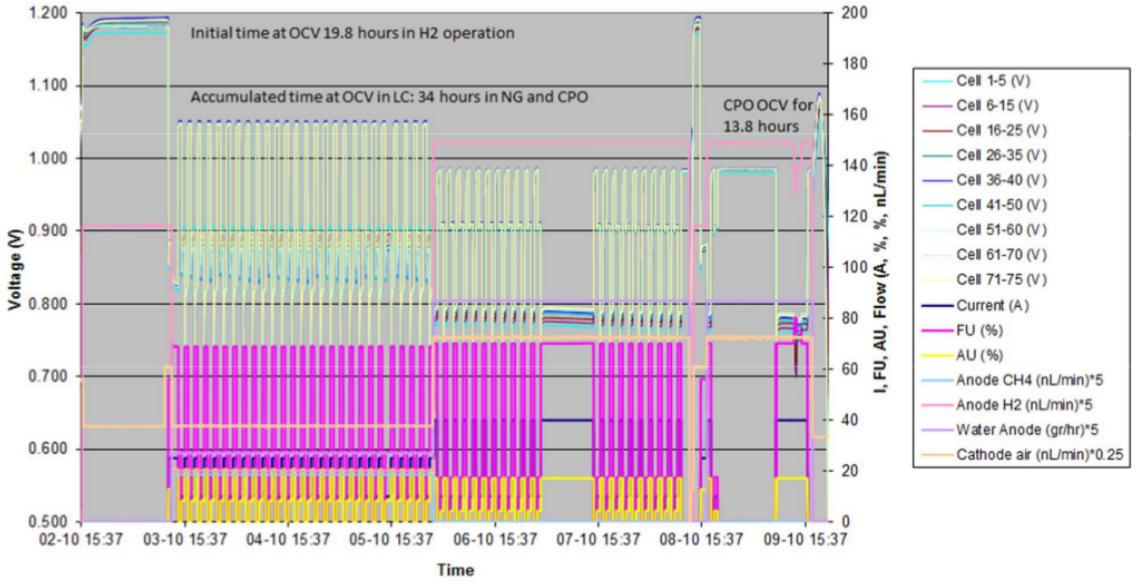

Figure 26: Data from extended multiple load cycle and OCV (idle operation) test carried out at TOFC.

[18]NG = natural gas (reformate), CPO = catalytic partial oxidation

Operating Mode	Suggested Goal Covered	Test & Results
Power burst	Partly, Time constraint of 5 sec up and down in 15 min. is covered.	CPO 10A to 40A sub second load cycles
Max Power	Partly	CPO 45A operation
Transient Up	Partly	1. CPO 10A to 40A LC e.g. 25% to 100% 2. NG 10A to 25A LC e.g. 40% to 100% with 95% performance in 2 min.
Transient Down	Verified	NG 25A to 0A LC, e.g. 100% to 0% with 95% stabilized value in < 1 min
Idle operation	Verified	1. For all tests reported above (>10) a minimum of 5x45 minutes at OCV was performed. 2. In a dedicated test 19.8 hours OCV in H_2, >34 hours of cycled 45 minute OCV periods in NG/CPO fuel and a full period of 13.8 hours at OCV was performed.
Cold start up	Not verified, although nothing indicating this cannot be done.	All tests reported here had a start-up time from cold to operating temperature in approximately 90 min. This was limited by the maximum heating rate of the test rigs available at TOFC.

Table 4: Summary of test data from TOFC stacks, this does not include data from tests using PowerCores. CPO = operation with a carbonaceous Catalytic Partial Oxidation fuel gas. NG = operation with reformed natural gas as fuel gas .

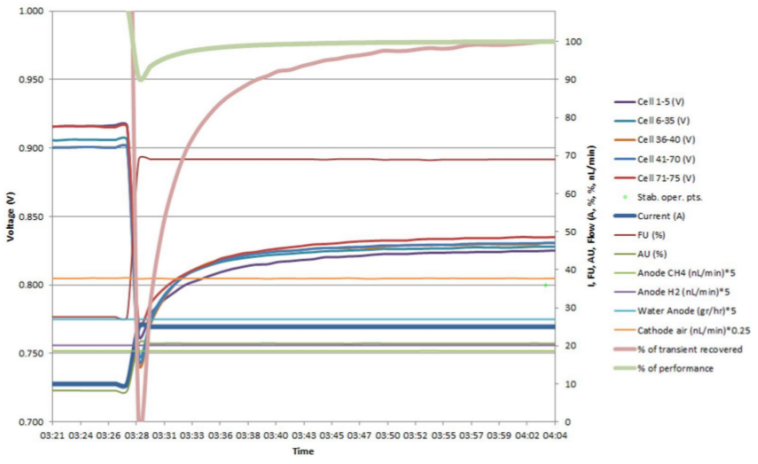

Figure 27: Transient response of a tested stack upon an abrupt load change from 10 to 25 A

1.3.4.2 Identification of Major Robustness Issues - A Statistical Approach As was illustrated by the previous section and the summary in WP1, it is clear that the current stack technology already shows good robustness with respect to most of the Smart Grid relevant parameters. However, in the project focus was placed on remaining areas where robustness was not adequate - especially on the issue that we describe as "Loss of Contact" inside the stack caused by harsh operating conditions and/or dynamic effects.

A large effort has been put into identifying and understanding the remaining key issues, which was

needed in order to improve the stack and be able to manufacture stacks of improved robustness (Milestone 4.2). The work conducted in this area was co-funded by the project "SOFC Accelerated" funded by EUDP (ENS-64012-0225), and comprised 55 different stack tests carried out after September 2012. Figure 28 shows the categorization of the "break down" issues found in these tests, and clearly shows why emphasis was placed on solving the "Loss of Contact" issue. Furthermore, as illustrated by figure 29, the distribution of the observed issues over the positions of the cells in the stack was also established in this study. The issues found were located throughout the stack, but with a bias against the outermost cells, where the mechanical and thermal issues have the largest impact. Dynamic Operating Conditions were further investigated in WT4.2 and to investigate which factors in stack production and testing that has the greatest influence on the stack robustness against Loss of Contact a series of hypotheses have been investigated by stack testing. The idea was to create Loss of Contact based on controlled, introduced weaknesses. If a certain weakness (change in components or process) resulted in a significant reduced robustness in the specific cell group, it indicates that one of the important factors of stack robustness has been investigated. This was a very comprehensive study including more than 17 stacks, each modified in a certain way to provoke errors leading to contact loss failure based on a number of different hypotheses.

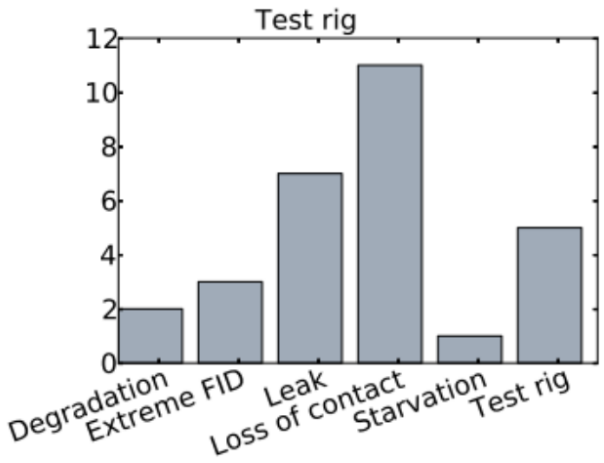

Figure 28: Number of observed issues in the studied series of stack tests broken down in six categories.

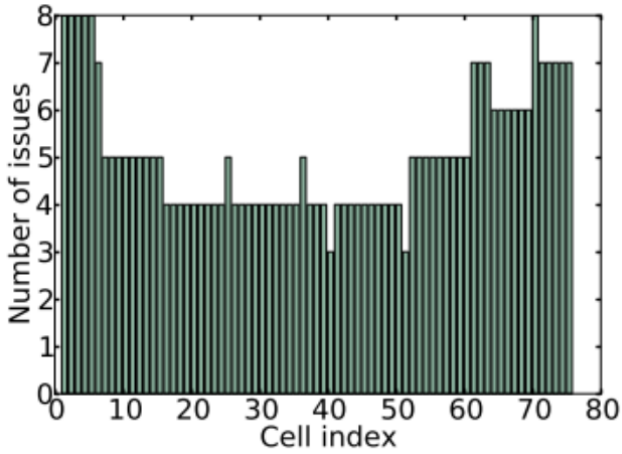

Figure 29: Location of cells with issues in tested stacks.

1.3.4.3 Improved Robustness Towards Loss of Electrical Integrity In the late spring of 2014, selected improvements developed in this and other projects were implemented in a production campaign consisting of 28 stacks.[19] A key feature of the evaluation of this production campaign is that it included a tough robustness test for all stacks, consisting of a thermal cycle and 5 load cycles (CH_4, 25A). The QA test profile and the QC points are illustrated in figure 30.

[19]The production campaign was largely funded by the EUDP sponsored project "SOFC Accelerated", ENS-64012-0225

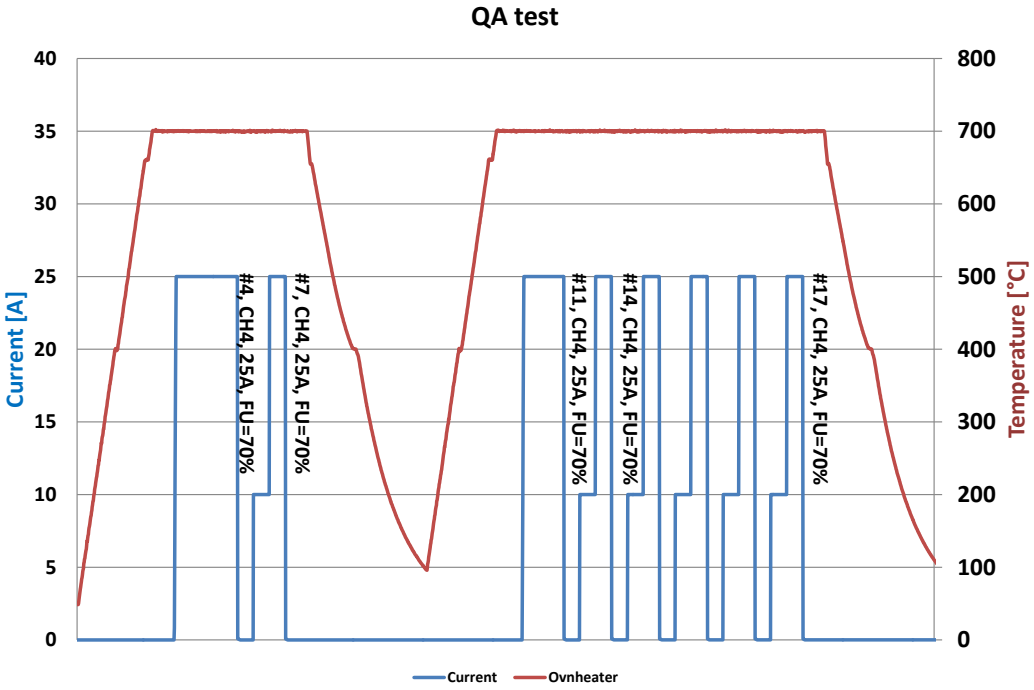

Figure 30: Quality Assurance (QA) test profile and Quality Control (QC) points. The frame drawn with a broken line highlights the included robustness test.

None of the tested stacks were rejected in the quality control. The observed average cell voltage change (dV) observed after the robustness test during the stack quality assurance testing for the 28 stacks resulting from the mentioned production campaign is displayed in figure 31. The large dV for stacks Q-557 to Q-560 is due to deviations in the test cycle. No serious robustness issues were discovered by the extended robustness test, and the campaign adds significantly to the confidence in the chosen and implemented stack improvements. It also confirms that the milestone *M.4.2: Demonstrate improved robustness of stack towards loss of electrical contact*, has been met.

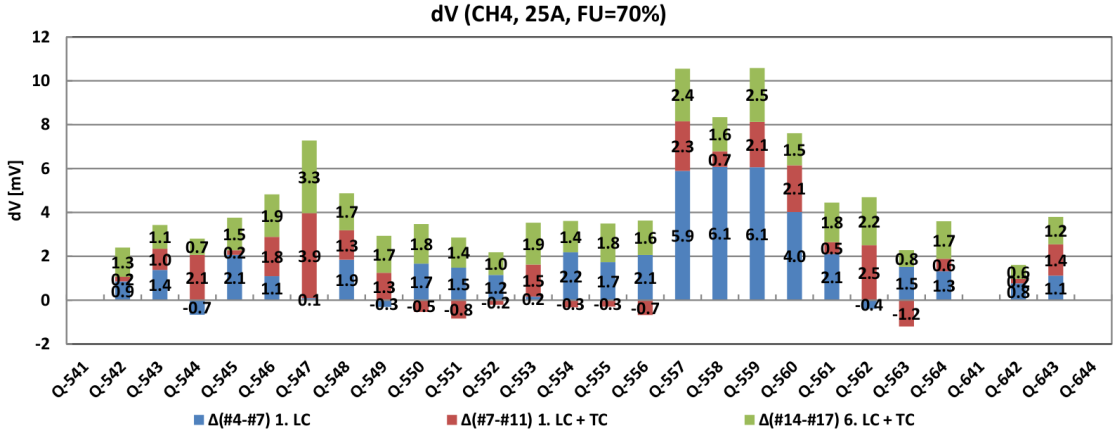

Figure 31: Overview of the voltage drop (CH_4, 25A, FU=70%). d(#4-#7) is the voltage drop after the standard load cycle, d(#7-#11) is the voltage drop after the thermal cycle and d(#11-#17) is the voltage drop after the 5 load cycles.

1.3.4.4 WT4.3 – Advanced In-situ measurements for Stack Testing

1.3.4.4.1 Spatially Resolved Thermal Probing In-situ temperature measurements were carried out in a stack with ten thermocouples distributed throughout a number of 75 cell stacks, each consist-

ing of three 25 cell blocks. The thermocouples were built in between two statotherm seals between two of the three 25 cell blocks, placed between cells 50 and 51. This enabled measurement of the temperature distribution across a cell in the stack during operation. The stacks were tested through the standard robustness tests and showed some issues probably related to leaks because of the segmentation of the stack. However, the performance was quite adequate for investigating the internal temperature profiles. The stacks were tested in a range of operating conditions in order to map the internal temperature profiles inside the stacks. The tests were performed at Smart Grid relevant conditions, also up to high current conditions ("Power Bursts"). The tests have given many useful results which has allowed TOFC to refine and calibrate existing modeling tools.

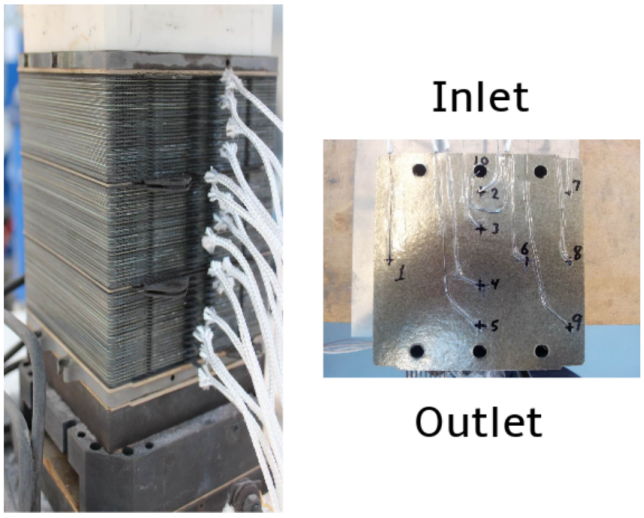

Figure 32: Photographs illustrating the 75 cell stack consisting of three 25 cell stack cores (left panel), and the temperature probe placement in between two cells (cells 50 and 51) in the stack (right panel).

The stack was tested through the standard robustness tests and showed some issues probably related to leaks because of the segmentation of the stack. However, the performance was quite adequate for investigating the internal temperature profiles. Figure 33 shows a heating gradient measured during a load cycle segment, when stepping the current load from 10 A to 25 A with CH_4 reformate fuel fed to the anode-side of the stack. For Smart Grid application and for general robustness of the stack it is evident that one important issue in regards to real life performance is the impact of changes in load. Standard tests at TOFC are designed to induce hard thermal stresses during load cycling, which the stack is designed to resist. However, with these tests it is now possible to see these phenomena, which so far was only visible in simulation models.

The stacks were tested in a range of operating conditions in order to map the internal temperature profiles inside the stacks also with constant operating conditions. The tests were performed at Smart Grid relevant conditions, also up to high current conditions ("Power Bursts") The tests have given many useful results which has allowed us to refine and calibrate the available modeling tools.

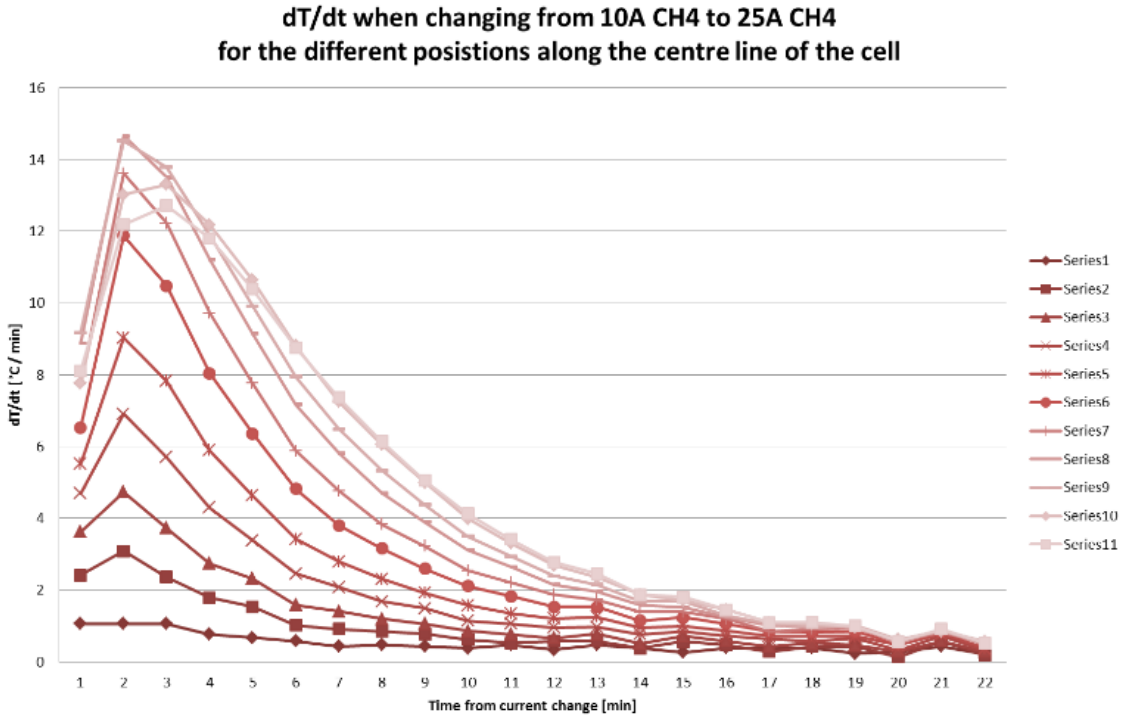

Figure 33: Temperature gradient observed across the cell during a load cycle, after step from 10 A to 25 A with reformate fuel fed to the anode-side of the stack.

Figure 34 shows how the temperature profile through the stack varies with fuel utilization. The stack will experience increased cooling from CH_4 reforming with lower fuel utilization, which is an important factor for the thermal gradients and thus mechanical robustness of the stack. These two stacks have also been used for investigating the influence of the boundary conditions for the stack in the form of surrounding temperature.

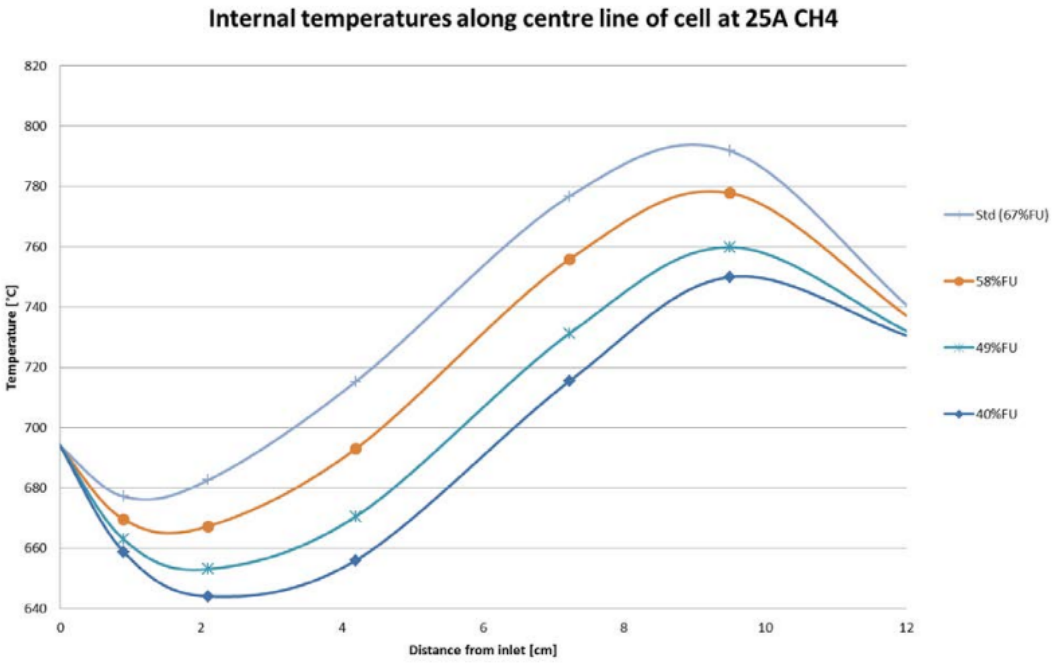

Figure 34: Temperature measurements along the flow path of a cell in a stack during operation at 25 A and with methane reformate fuel gas as a function of fuel utilization (i.e. at varying fuel flow rates).

1.3.4.4.2 Detailed Impedance Measurements of Short Stacks In-situ characterization of SOFC stacks have so far largely been limited to measurements of the voltage from interconnect to interconnect, *i.e.* measurements from the individual cell voltages or even the summed voltage from groups of cells. This work task had as it aim to significantly advance the tool set for in-situ SOFC stack diagnostics

by development of improved methodology for diagnostics of technological stacks. A significant effort was placed on implementation of a measurement set-up using parallel impedance acquisition equipment, allowing simultaneous acquisition of impedance spectra for a whole stack and up to 16 repeating units or cell blocks in the stack, and integration of this equipment with an existing stack test stand. This effort was carried out in conjunction with a concurrent PhD project on the topic of "SOFC Stack Diagnostics" supported by Copenhagen Cleantech Cluster and the results and methodology developed here was further used in the project "SOFC Accelerated" supported by EUDP (ENS-64012-0225) where it was used to study the relatively fast initial degradation period often observed in SOFC stacks. A stack was tested using an automated test rig purchased from FuelCon AG, and characterized using Electrochemical Impedance Spectroscopy (EIS). An illustration of the EIS test set-up is shown in Figure 35.

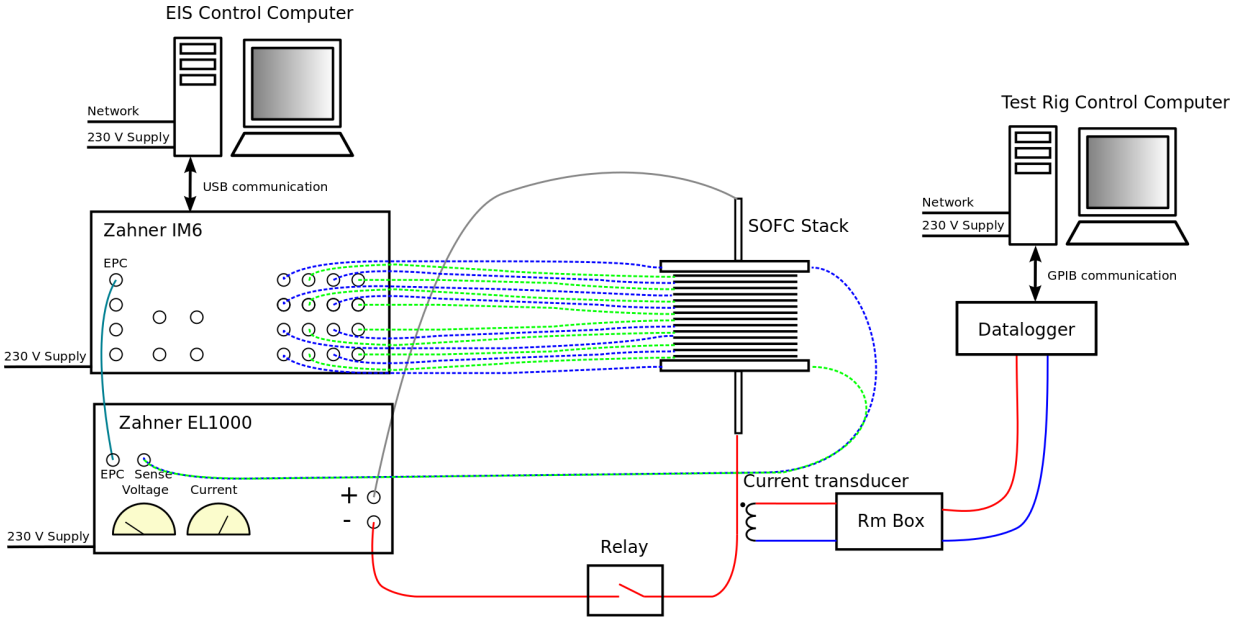

Figure 35: Illustration of the test set-up for EIS measurements on SOFC stacks.

The test rig computer controls the EIS computer via a network connection. The EIS computer controls the Zahner IM6 Potentiostat via a USB connection. The Zahner IM6 controls the Zahner EL1000 Electronic Load via an EPC connection. In combination the Zahner IM6 and the Zahner EL1000 can record EIS measurements of the stack and 16 RUs simultaneously. The DC current is measured by a current transducer and the data is logged by the test rig control computer via a data logger. A relay is implemented in the set-up in order to disconnect the Zahner IM6 and the Zahner EL1000 if the cell voltages exceed over- or undervoltage limits. The complete test set-up is fully automated. EIS measurements were recorded on 14 RUs and the stack simultaneously.

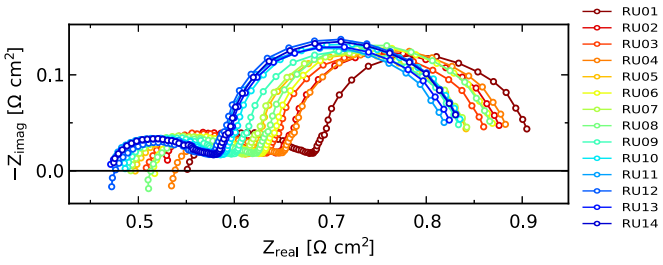

Figure 36: Simultaneously collected EIS spectra for the 14 RUs in the stack measured at 700°C. Fuel: 20% H_2O and 80% H_2 Oxidant: Air

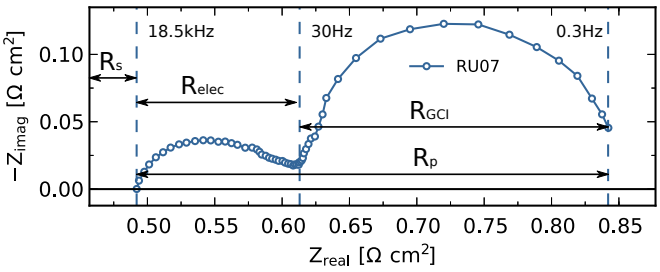

Figure 37: Impedance spectra for RU07 at 700°C Fuel: 20% H_2O and 80% H_2 Oxidant: Air. The series resistance, Rs, is extracted at 18.5 kHz, the polarization resistance, Rp, is extracted between 18.5 kHz and 0.3 Hz. The gas conversion resistance, RGCI, is extracted between 30 Hz and 0.3 Hz.

It was demonstrated that with the improved placement of current feeds and voltage probes it is possible

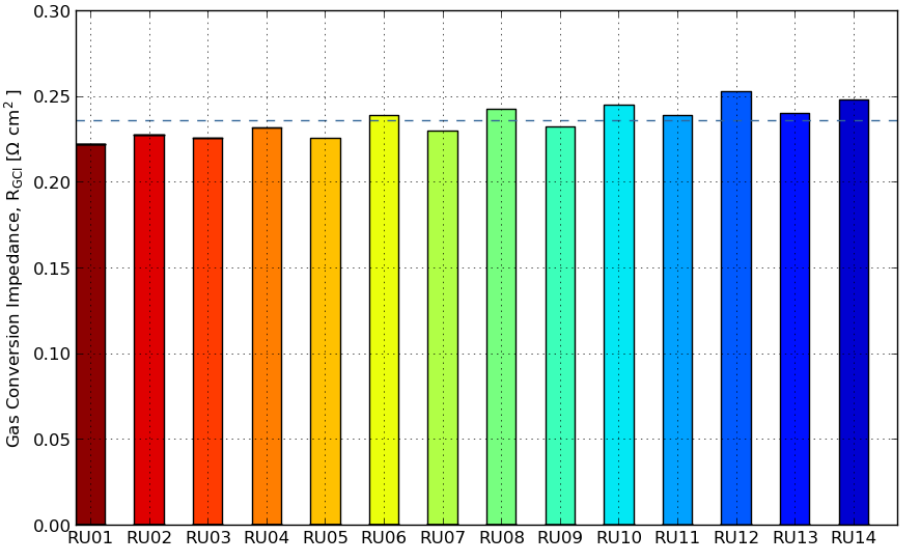

Figure 38: Gas conversion resistance, R_{GCI}, vs Repeating Unit (RU) at 700°C. Fuel: 20% H_2O and 80% H_2 Oxidant: Air. The dashed line represents the average gas conversion resistance.

to separate the different contributions to the internal resistance of the stack into an ohmic and a polarization part and that the low frequency response (the gas concentration impedance) is useful in detecting mass transfer limitations. This methodology can be used to detect possible minor changes in the supply of gas to the individual cells, which is important when going to high fuel utilizations. The fuel flow distribution provides important information about the operating limits of the stack when high electrical efficiency is required. Figure 36 displays impedance spectra recorded of the 14 repeating units of the tested stack, and figure 37 illustrates the basic parameterization of the impedance response into the parameters R_s (Ohmic resistance), R_{elec} (electrode polarization resistance), and R_{GCI} (the gas diffusion and conversion impedance). The observed series resistance decreases from bottom (RU01) to top (RU14) by 16%. Estimating the expected temperature difference using a simple Arrhenius expression and the observed activation energy of R_s, the difference should be 12%. Thus, the trend in R_s is reflecting the gradient in average RU temperature across the stack. Furthermore, the fuel flow distribution in the stack is reflected in the variation of the R_{GCI} across the stack. The difference between the lowest R_{GCI} from RU01 and the highest R_{GCI} from RU12 is ~12%. The general trend is that R_{GCI} increases with increasing RU. An estimate using simple theoretical expressions for the gas conversion resistance with a measured temperature difference on 12°C between top and bottom of the stack shows that the difference should be ~1% if it was a pure temperature effect, which means that most of the observed variation in RGCI is due to differences in the fuel flow rate at the across the RUs in the stack. The data indicates that slightly less fuel is supplied to the top of the stack compared bottom of the stack. Figure 38 illustrates the variation of RGCI across the stack.

In summary, the activities in WT4.3 has significantly advanced the available toolset and possibilites for detailed and spatially resolved temperature and performance measurements.

1.3.5 WP5 - Mechanical Properties of Critical Interfaces and Layers

The mechanical properties of components and interfaces in the cell and single repeating units were addressed in the work package. The work initially concentrated on screening of experimental techniques and production of samples that as closely as possible would reflect real interfaces in SOFC stacks and cells.

The adhesion (reflected in the interfacial fracture energy release) between different layers, *e.g.* electrolyte / cathode and cathode / current collector is of particular interest since the perovskite materials used in the cathodes of this project (LSCF, LSC) have relatively high thermal expansion coefficients, and therefore need to be firmly anchored on the half-cell in order to prevent delamination when exposed to thermally induced stresses.

Two milestones were defined for this work-package: M5.1 – "Quantification of adhesion and cohesion of two different cathode side layers" and M5.2 – "Quantification of anode-side adhesion". Both milestones

are considered to have been reached, based on the experimentally obtained bonding strengths, mainly from three-point bending studies.

The main problem with mechanical testing and quantification of interfacial mechanical properties in solid oxide cells and repeating units (stacks) is to prepare samples and find techniques that allows the right interfaces to be addressed. This has forced the work into two main directions:

1. the use of nano/micro indentation techniques to probe the mechanical properties in and around interfacial areas in polished cross-sections of prepared samples (mainly for electrolyte/barrier/cathode interfaces)
2. the use of a three-point bending technique which was adapted from the ISO 9693 Schwickerath test which was found to be a suitable technique for the determination of the bonding strength in solid oxide cell - interconnect interfaces.

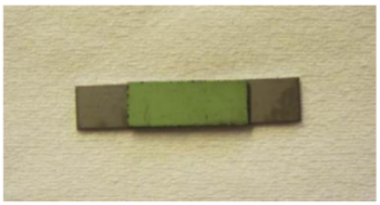

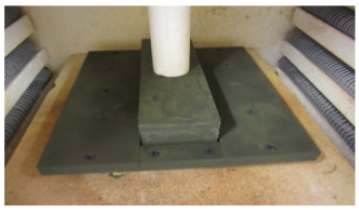

Load: 0.5-2 kg/cm^2
Firing: 910°C/24 hs
Reducing and oxidizing conditions

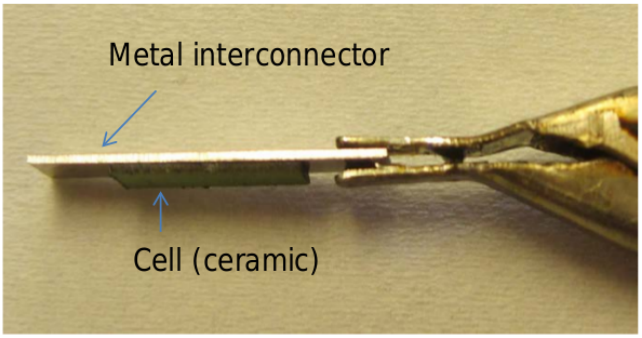

Figure 39: Photographs illustrating the sample preparation of the interconnect - anode support samples for investigation of the anode - interconnect adhesion.

1.3.5.1 WT5.1 Quantification of Cathode Layer Adhesion and Cohesion Modulus mapping and quasi-static nano-indentation were used to determine the mechanical properties within polished cross-sections of two electrolyte (CGO) supported cathode (LSC-CGO) specimens sintered at 850°C and 1050°C, respectively. In particular, the electrolyte / cathode layer interfacial regions of the samples were investigated. The main results were the successful determination of the elastic modulus of the CGO electrolyte and the composite LSC-CGO cathode layer. Furthermore the effect of sintering (particle coarsening, improved interparticle necking) on the mechanical properties was determined. An increase of the sample sintering temperature led to a higher Young's modulus for LSC/CGO sample from ~81 to 134 GPa. For the CGO electrolyte (dense) there was no appreciable change with sintering (as expected): the value remains between 215-225 GPa. Typical reported values for Young's modulus of (dense) NiO and YSZ are ~ 220 GPa. Dense samples of LSC ($La_{0.6}Sr_{0.4}CoO_{3-\delta}$) and LSCF ($La_{0.6}Sr_{0.4}Co_{0.2}Fe_{0.8}O_{3-\delta}$) have been reported to display a Young's modulus of approximately 165 GPa (LSCF) and 135-40 GPa (LSC). [20][21][22]

Figures 40 and 41shows images of the examined cathode cross-section and the indentation pattern used.

[20] Liu, X. et al; "Strength of Highly Porous Ceramic Electrodes " J. Am. Ceram. Soc., 2011, 1-9.
[21] Giraud, S.; Canel, J.; "Young's modulus of some SOFCs materials as a function of temperature " Journal of the European Ceramic Society 28 (2008) 77–83
[22] Kimura, Y. et al; "Mechanical Properties of $La_{0.6}Sr_{0.4}Co_{1-y}Fe_yO_{3-\delta}$ under Various Temperatures and Oxygen Partial Pressures" ECS Transactions, 35 (1) 2429-2434 (2011)

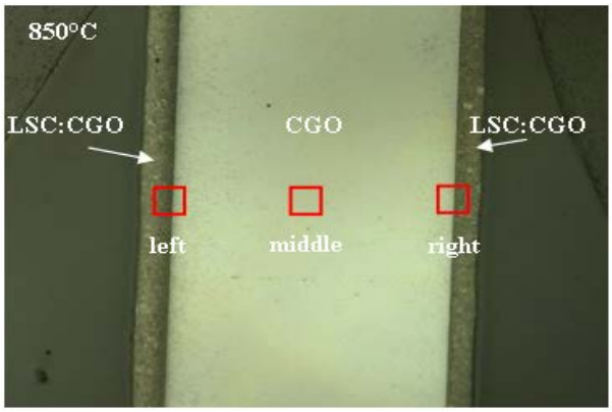

Figure 40: Micrograph showing the structure of the LSC-CGO / CGO / LSC-CGO samples.

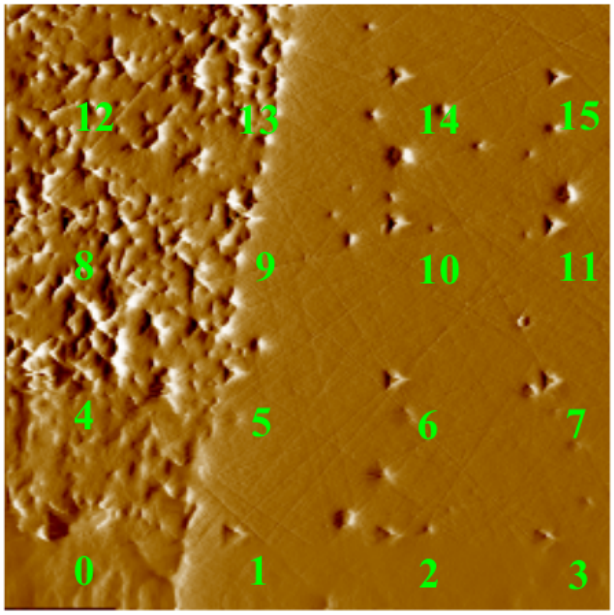

Figure 41: AFM image showing the indentation pattern used for the nano-indentation study.

Different loads were applied during indentation testing from the nano-range 1000 μN, up to 1.5 N. However, no crack propagation through the (CGO) electrolyte / cathode interface was detected. Cracks kink to the cathode side since the fracture toughness of the cathode is lower than the interfacial fracture toughness. This crack propagation behavior makes difficult to employ the interfacial indentation test, since one of the parameters required to determine the interfacial fracture toughness is the size of a interfacial crack for a given applied load. Therefore, in order to assess interfacial bonding strength, three point bending testing was performed with a thermo-mechanical analyzer (TMA) in accordance with EN ISO 9693-1 standard, which is a test used to assess metal-ceramic compatibility. Residual stresses were also calculated by finite element modeling analysis.

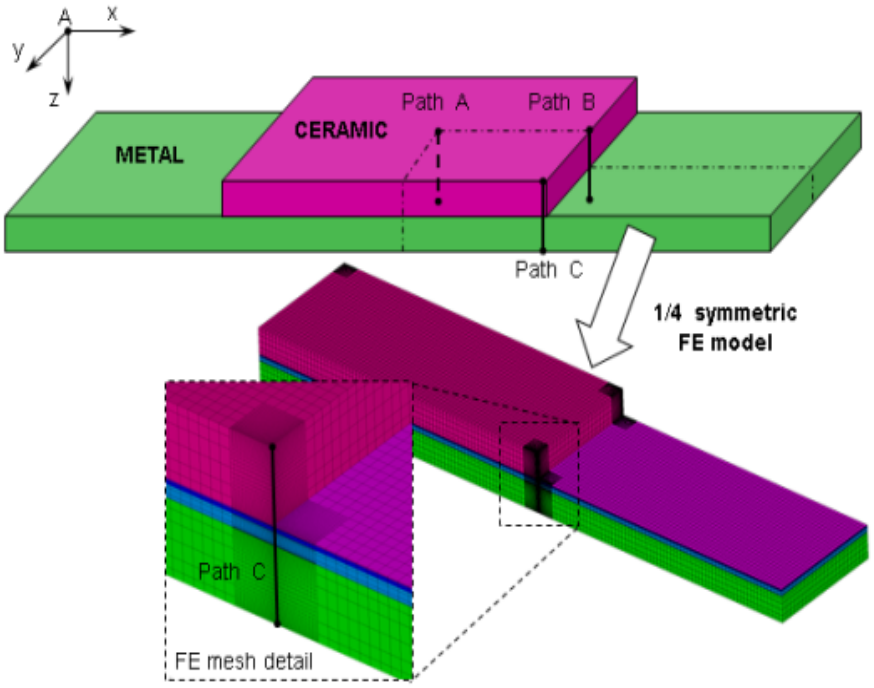

Figure 42: Schematic of the FE model for the calculation of residual stresses (on path A, B, C) and detail of the FE mesh.

It is clear that the highest stress concentration exists at the interconnect- ceramic interface. A set of

samples in which different cathode layer / interconnect interfaces were formed were tested using the three point bending technique. Even if the results may be influenced both by materials properties and the slightly varying degree of interfacial contact area in the different samples, it was demonstrated that the technique allows separation of the different samples, as illustrated by the results shown in figure 43. This work corresponds to fulfilment of milestone 5.1: "Quantification of the adhesion and cohesion of two different cathode-side layers completed".

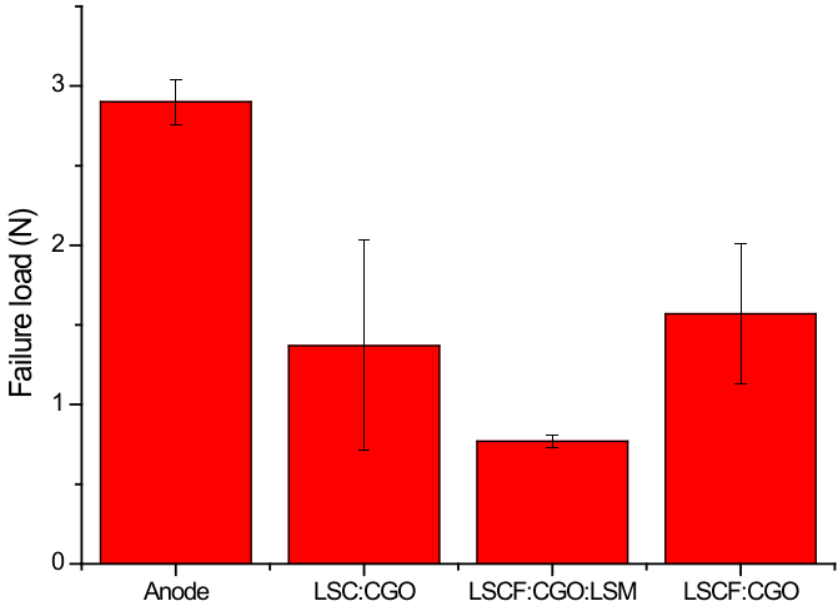

Figure 43: Measured interfacial failure loads for four sets of samples with different ceramic / cermet layer - interconnect interfaces.

1.3.5.2 WT5.2 Strength of Anode / Interconnect Interfaces The same experimental approach employed for the assessment of bonding strength in cathodes was applied to study the anode-interconnect interface. Figure 44 shows the stress distribution along path C in the anode-interconnect specimens for the case of combined loading. The anode bonding strength shows the strongest bonding to the interconnect as compared to the cathode interfaces in case of pure mechanical loading (figure 43). The residual stresses are also the lowest in this case, due to the good agreement between the thermal expansion coefficients of the materials forming this interface.

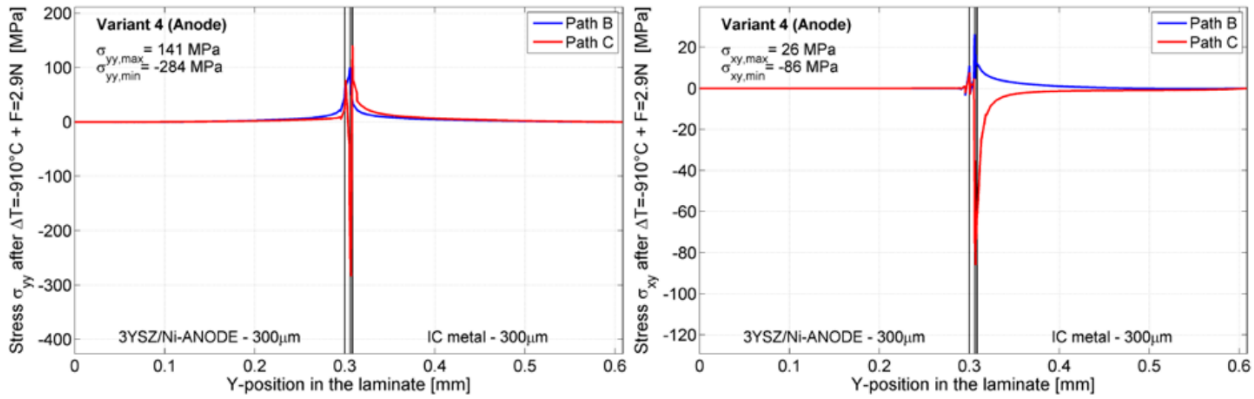

Figure 44: Stress distribution along path C in the anode-interconnect specimens for the case of combined loading

SEM and EDS analyses were also carried out to study the chemistry of the interface. In the case of the anode-interconnect interface, the bonding mechanisms are different than in the case of the cathodes, i.e. this is a metal-metal bonding. Both Ni and Co remain in the metallic state in the reducing conditions that sample was exposed to. From the elemental maps particles containing Cr, Co, Fe, Ni can be found close to the interface. These are intermetallic particles formed by the diffusion that ensure good bonding of the anode to the coating and the interconnect.

The fracture toughness of the anode support material (Ni-3YSZ) is higher than the interfacial toughness between anode support and metal interconnect, and hence the fracture energy is employed to break the bonds between metallic Ni (from the reduced anode support cermet) and the metal interconnect. It is important to note that the reaction sintering treatment used in the sample preparation was performed in reducing conditions (9% H_2/N_2) and hence, as expected, no oxides formed on the metal interconnect. The crack propagates through the interface and no crack kinks to the anode cermet were found. This work completes milestone 5.2: "Quantification of the anode-side (anode / interconnect) adhesion completed ".

1.3.6 WP6 - Cell Components

This work package was focused on improving the cell performance, robustness, and durability of critical cell components with focus on components for operation at temperatures below 750 °C, and industrially relevant and up-scalable manufacturing techniques, e.g. screen-printing and tape-casting.

1.3.6.1 Physically Robust Cathode Layers

The work on increased robustness cathodes was reduced to a smaller effort in the project as the initial work in WP5 indicates that cathode – interconnect interface is a much weaker interface than the cathode – barrier layer interface is. A series of cells with LSC-CGO cathodes of varying microstructure were produced and delivered for testing. However, milestone M6.1 is considered not fulfilled, as this only provided a possibility to evaluate variations in cohesion in such a cathode and also the interfacial adhesion between barrier and cathode, but no cell with a more robust cathode layer was manufactured and delivered for testing. The evaluation of the mechanical properties of the cathode was described above in 1.3.5.1.

1.3.6.2 Improved Cell Components A large part of the cell resistance observed in 2.5G type cells at temperatures below 750 °C originate from the electrolyte and barrier layer of the cells, and are to some extent due to current constriction effects caused by non-optimal electrode / electrolyte interfacial coverage, and from resistive reaction products (secondary phases, solid solution formation) at the barrier / electrolyte interface. Improvements of the electrode design was explored primarily by reducing the particle size in the anode layer. Tape-cast, laminated, and co-fired barrier layers of various thicknesses were investigated and compared with barrier layers produced by PVD.

Further, tape-cast and laminated half-cells with a thinner electrolyte layer (4-6 µm) were produced and delivered for testing. These cells formed the main part of the tested cells in the project. A cell with a fine anode (smaller particles in the anode layer) was produced and delivered for testing and together with the batch of half-cells with thinner electrolyte corresponds to fulfilment of milestone 6.2: "An improved cell developed and delivered for testing". A separate study involving the evaluation of cells with very thin electrolyte produced using ink-jet deposition was also carried out. Together, these studies provide a number of protocols for preparation of cell components with a decreased resistance.

As the LSC-CGO cathode developed in the project "Durable and Robust SOFC" (ForskEL 2010-1-10441) performs very well, and yields a low resistance compared with other cell components investigated in this project, this electrode was kept as the main oxygen electrode throughout the project.

Another important topic was the investigation of Ni-ceramic wetting and agglomeration properties, using a model system consisting of relatively flat ceramic surfaces (polished dense pellet surfaces) of YSZ and ScYSZ, respectively, onto which NiO was evaporated and later reduced. This study has provided new experimental methodology that yields information about the Ni-ceramic interactions and agglomeration in the different model systems.

The exploration of infiltration of electrodes for improved impurity tolerance and performance enhancement was also undertaken and was reported in 1.3.3.2.2.

1.3.6.2.1 Manufacturing and Evaluation of Co-fired Tape-Cast Barrier Layers In order to reduce cost and simplify production, it is attractive to employ techniques such as multilayer tapecasting, that allows shaping of most or all of the cell in a single step, followed by a single sintering step. In this project a two step shaping and sintering route was explored, encompassing a first step in which the half-cell (including the barrier layer) is tape-cast, and sintered, followed by a second step in which the oxygen electrode (SOFC cathode) is applied by screen-printing and subsequently sintered. This removes the separate shaping and firing step associated with application of screen-printed or sprayed

barrier layers. In this effort the potential of this strategy is explored while attempting to find the lower limit for the resistance of the resulting barrier / electrolyte bilayers (reflected in the series resistance of a cell). A series of cells with varying thickness and porosity of the barrier layer were tested. Figure 45 shows a collection of micrographs that illustrates the thickness and porosity variation among the samples, and the test results are summarized in figure 46. The co-sintered barrier layers produced a significantly greater ohmic resistance than the layers deposited using PVD, most likely due to solid solution formation at the electrolyte-barrier interface in the former case.

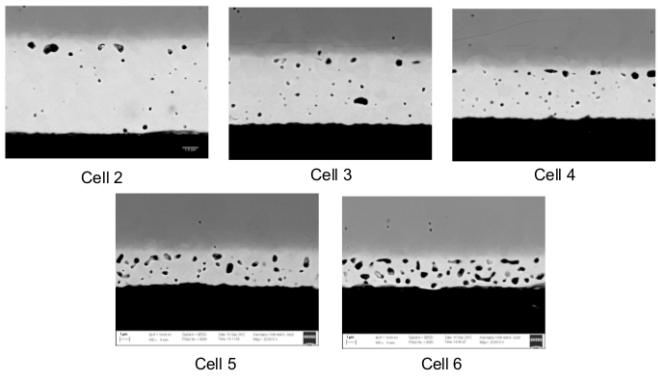

Figure 45: SEM micrographs showing the structure of the CGO barrier layer (brightest phase) incontact with the electrolyte (8YSZ) in cells 2 - 6. As the thickness of the layer decreases the porosity of the layer increases somewhat.

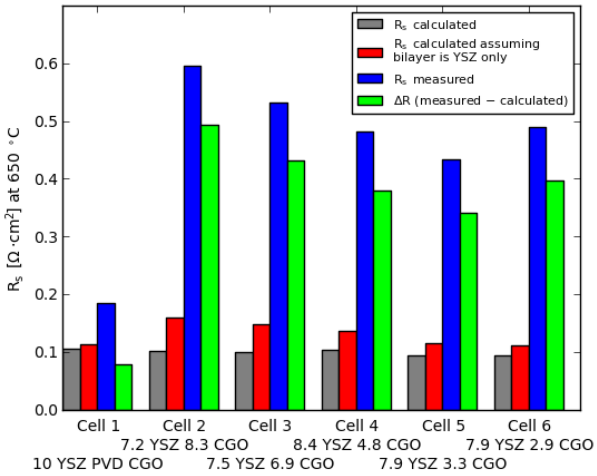

Figure 46: Summary of calculated and observed area specific series (ohmic) resistances for the tested cells. All measurements were carried out at 650 °C with a hydrogen - water fuel gas mixture and air as the oxidant.

1.3.6.2.2 Tape-Cast (Half-)Cells with Thin Electrolytes and Reduced PSD Anode Layer Tape-casting and lamination was further employed to investigate cells with variations in the Ni-content in the anode, a modified anode with smaller particles, and thinner electrolytes (4-6 µm). It was shown that cells with finer anode could be produced using two different routes, and electrolytes down to ~4 µm in thickness could be produced as a standard in the project. As the co-fired barrier layers investigated in 1.3.6.2.1 yielded a relatively high series resistance, the remaining cells in the project were provided with barrier layers produced by PVD after the half-cell was sintered.

The cell with a finer anode (Cell B) was tested in WP3 (1.3.3.3.2) and was found to exhibit a lower anode polarization resistance and thus lower anode overpotential at comparable currents than the other, coarser, anode layers used in the other cells tested in the project. The thinner electrolyte layer in Cells A and B also yielded a lower ohmic resistance than that observed for cell C, consisted with the differences in electrolyte thickness (table 2). Figure 47 and 48shows SEM micrographs of two cells corresponding to Cell A and B in table 2, that were produced in the project.

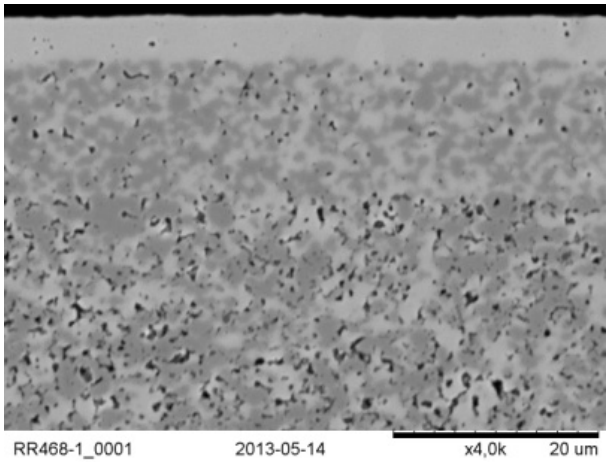

Figure 47: SEM micrograph of a half-cell corresponding to that in Cell A in table 2.

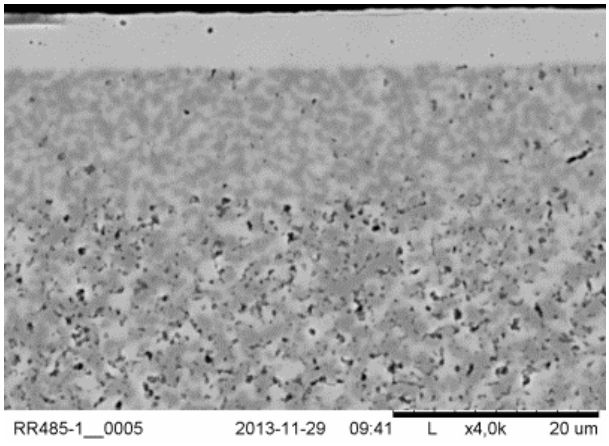

Figure 48: SEM micrograph of a half-cell corresponding to that in Cell B in table 2.

1.3.6.2.3 Ink-jet Deposited SOC Functional Layers A cell with a YSZ electrolyte of approximately 1.2 µm thickness was produced using ink-jet printing to deposit a colloidal suspension of YSZ onto a Ni-YSZ anode + anode-support. The half-cell was fired and subsequently a LSM-YSZ cathode, and a LSM current collection layer, deposited and fired in a separate steps in order to prepare the cell for performance testing. The cell was manufactured in collaboration with an internal project, where "Towards Smart Grid Ready SOFC" contributed in the areas of ink development and cell testing. As the electrolyte bilayer (YSZ electrolyte + CGO barrier layer) of modern anode-supported SOFCs is a large contribution to the internal resistance of the cell at lower operating temperatures this is a step on the way to improving the performance of the anode supported SOFC. One of the key questions in this test was to examine whether satisfactory leak tightness of the very thin electrolyte layer had been obtained, which was assessed in the test by monitoring the cell voltage as a function of the fuel flow rate. The observed cell voltage was compared with the theoretically expected cell voltage and the leak was quantified in terms of an equivalent leak current.[23] The leak test data obtained is shown in figure X and the polarization curves recorded in the temperature interval 850 - 650 C are shown in figure XX.

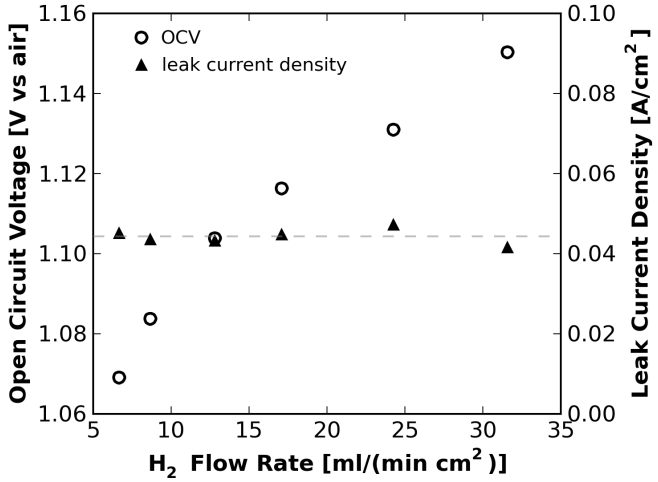

Figure 49: Observed open circuit cell voltage (open circles) and calculated total leak current density (filled triangles) of 5-layer electrolyte SOFC operates with dry hydrogen supplied as fuel at the indicated flow rates and air as the oxidant. The dotted horizontal line represents the average leak current density (0.044 A cm^{-2}), calculated using the active area of the cell (= 16 cm^2).

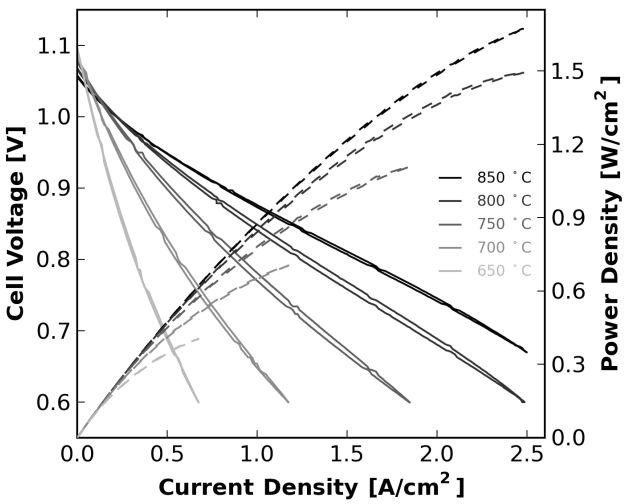

Figure 50: Polarization curves recorded at different temperatures for the cell with the ink-jet printed electrolyte. The fuel was 96% H_2 and 4% H_2O supplied at a total flow rate of 26 ml min^{-1} cm^{-2}and the oxidant was air.

1.3.6.2.4 Ni agglomeration and wetting behavior on YSZ and ScYSZ The agglomeration and wetting behavior of Ni on different zirconia substrates is interesting because both influence the mi-

[23] J.F.B. Rasmussen, P. V. Hendriksen, A. Hagen, Fuel Cells 8 (2008) 385-393

crostructure and performance of the cermet anodes after reduction. In real anodes the reduction can lead to very different results depending on the dopant in the zirconia, *i.e.* if it is yttria stabilized zirconia (YSZ, Y), or scandia and yttria co-doped zirconia (ScYSZ, S). Model systems are ideal to study due to a simplified geometry. Model samples of NiO thin films on sintered YSZ and ScYSZ substrates with different treatments were reduced and the resulting microstructure was studied with scanning electron microscopy (SEM) and atomic force microscopy (AFM). It is well known that Ni will de-wet the zirconia. Automatic image analysis was used to quantify a large number of particles and an agglomeration factor (1, 2) was calculated. The calculated apparent contact angle[24,25] was compared to actual contact angles measured from cross sectional SEM images. All substrates were pressed and sintered for 4 h at 1500°C to get dense samples and then subsequently polished. This resulted in samples "P-Y" and "P-S". Some of the polished samples were heat treated for 10 h at 900°C and this resulted in samples "H-Y" and "H-S". Heat treatment causes a thermal etching of the surface and also induces segregation of impurities to the surface. NiO thin films were deposited on all samples by pulsed laser deposition with a resulting thickness of ca. 200 nm. The samples were then reduced in 9 % H_2 in N_2 with 1 % H_2O at 900 °C for 2 h.

The samples were investigated (without carbon coating) in low-voltage SEM and Figure 51 shows the resulting morphology of the Ni. Significant differences depending on the substrate were found. H-Y showed facetted particles, many of them elongated. P-Y shows a semi-network and only a few single particles. The network structure consists of long rows of interlinked particles with multiple branches. It is clear that the particles do not favor a position on the grain boundaries. There are some indications that the pattern of the Ni particles is different on the different YSZ grains, *i.e.* the crystallographic orientation influences the agglomeration behavior. P-S and H-S show a very pronounced network structure and it varies from ScYSZ grain to ScYSZ grain, from an open network to an almost completely covering layer of fine-grained Ni. The height of the particles is generally in the range of 400-900 nm, and in the areas where Ni is covering the surface it is around 250 nm. Image analysis of the particles on H-Y was used to get information on a large number of particles and their surroundings and the agglomeration factor was found.

With AFM the diameters and height of 50 particles were measured and the apparent contact angle was calculated. A focused ion beam in an SEM was used to make cross sections of the particles to directly measure contact angles. Figure 52 shows the resulting cross sections and the table (figure 53) shows some of the measured and calculated parameters. The main result is that particles at least down to a few hundred nanometers in diameter are facetted, and that the contact angle is not size dependent, at least not for particles with diameters above 500 nm.

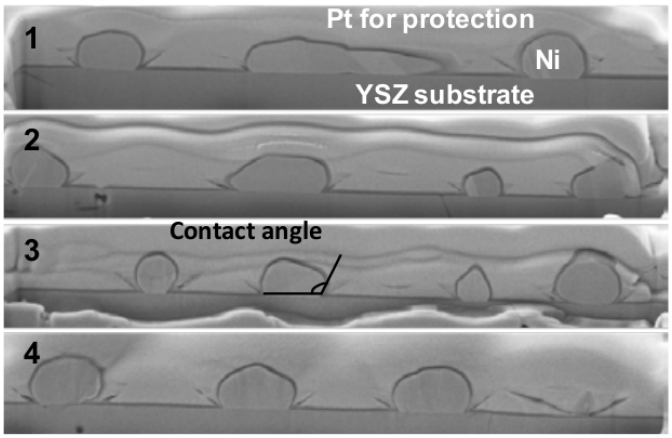

Figure 52: Cross sections of the Ni particles on H-Y made by FIB-SEM.

Parameter	Method	Value
Average particle height	AFM	630 nm ± 110 nm
Average aspect ratio	SEM	1.67 ± 0.65
Average particle diameter	AFM	2.0 µm ± 0.5 µm
Agglomeration factor	SEM, IA	4.22
Calculated apparent contact angle	AFM	65º
Average measured contact angle	FIB-SEM	130º

Figure 53: Table with the most important calculated or measured parameters for the H-Y sample.

First, it can be concluded that the NiO film was too thick, and this resulted in either the too large, elongated particles with facets or the network structures, where the film did not break up into particles. This interfered somewhat with the purpose of the analysis since the calculation of apparent contact angle assumes spherical – or at least close to spherical - particles. When this is said, the results are

[24]H. Kishimoto, A. Suzuki, T. Shimonosono, M. E. Brito, K. Yamaji,T. Horita, F. Munakata, H. Yokokawa, Agglomeration behavior of nickel particles on YSZ electrolyte, Solid State Ionics 225 65-68 (2012)

[25]H. Kishimoto, A. Suzuki, T. Shimonosono, M. E. Brito, K. Yamaji,T. Horita, F. Munakata, H. Yokokawa, Agglomeration behavior of nickel particles on YSZ and TiO2-doped YSZ, J. Power Sources 199 174– 178 (2012)

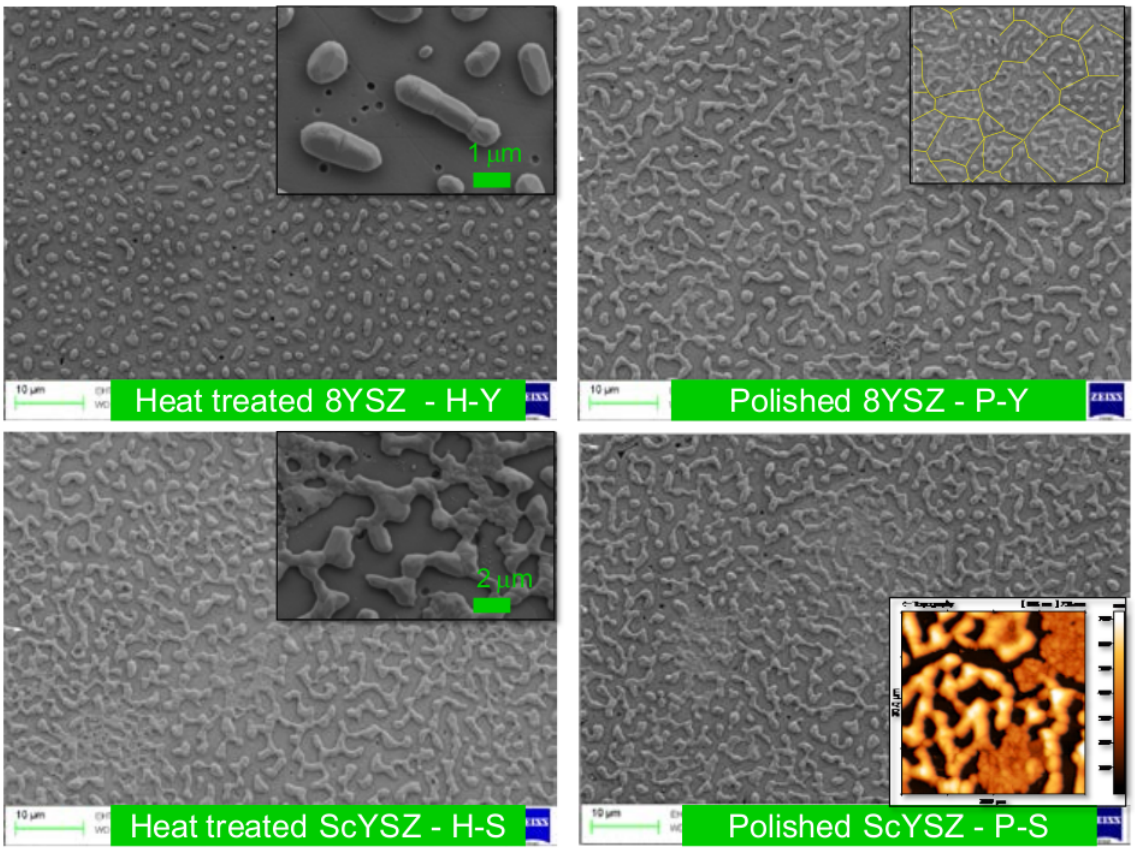

Figure 51: SEM images showing the different morphologies of Ni depending on the substrate type. H-Y shows facetted Ni particles. P-Y shows a Ni network, where the morphology depends on the substrate grain properties. The inset shows an attempt to draw the grain boundaries. H-S and P-S show longer Ni network chains and a more distinct difference in Ni morphology between some substrate grains. The insets show large, connected Ni grains on some substrate grains and much smaller Ni grains with a better coverage in other grains, and that the height of the latter is much lower than the height of the larger particles.

still very interesting as the calculated apparent contact angle (based on AFM measurements) was 65 ° for H-Y and this is close to the result from Kishimoto where the angles were ~70-80° for polished YSZ, Ti-YSZ and NiO-doped YSZ. Compared to these angles, the contact angle directly measured (using FIB-SEM) on the Ni particles is in the order of 130° and this significant difference leads to the conclusion that either the apparent contact angle is not a good measure of the actual contact angle, or the obtained particles exhibited a shape too far away from the ideal (round) shape. Smaller particles near the edge, where the original NiO films were thinner were subsequently investigated, and they also showed wetting angles considerably larger than 90°. The actual contact angle of ~130° still suggests that wetting of the Ni particles on YSZ is not favorable. Contact angles >90° corresponds to low wettability. The wetting and agglomeration behaviour on ScYSZ appears significantly different than on YSZ, but needs to be examined using thinner NiO films to allow quantification using the methods investigated here (at least for agglomeration factor determination, an interesting quantity for stability considerations).

1.3.7 Environmental Benefits of the Project

Denmark is committed to contribute to limit the global climate change as agreed in Copenhagen 2009 and in Cancún 2010. One integral part of this commitment is the reduction of greenhouse gas emissions in Europe by 80 - 95% in 2050 compared to the 1990 level. This project contributes to achieving this goal by carrying SOFCs further to a technology break through, where the inherent advantages of SOFCs can be utilized:

- Decrease the emission of CO_2 due to the higher system efficiencies
- Easier and cheaper carbon capture and further processing, as CO_2 is produced in concentrated form and not diluted by large amounts of air
- Avoidance of NO_x and SO_2 emissions, as these compounds are not formed in the SOFC process Ability to convert biomass to electricity with high efficiency. An additional outcome of this project

is related to the focus on smart grid integration of SOFCs, where sustainable energy technologies such as wind power, electrolysis, etc. are combined with each other for the benefit of environment and curb of global climate changes.

1.3.8 Publications and Patents

1.3.8.1 Publications

1. A.J. Samson, M. Søgaard, P. Hjalmarsson, J. Hjelm, N. Bonanos, S.P.V. Foghmoes, et al., "Durability and Performance of High Performance Infiltration Cathodes", Fuel Cells. 13 (2013) 511–519. doi:10.1002/fuce.201200183.
2. "Ceramic Fuel Cells for Sustainable Energy" – non-peer-reviewed popular presentation of the projects "Durable and Robust SOFC" (ForskEL 2010-1-10441) and "Towards Smart Grid Ready SOFC" in the journal "International Innovation", December 2012, published by Research Media Inc, Bristol, United Kingdom (not peer-reviewed).
3. T. Ramos, M. Søgaard, M.B. Mogensen, "Electrochemical Characterization of Ni/ScYSZ Electrodes as SOFC Anodes", J. Electrochem. Soc. 161 (2014) F434–F444. doi:10.1149/2.045404jes.
4. J. Nielsen, J. Hjelm, "Impedance of SOFC electrodes: A review and a comprehensive case study on the impedance of LSM:YSZ cathodes", Electrochimica Acta. 115 (2014) 31–45. doi:10.1016/j.electacta.201
5. A. Hauch, A. Hagen, J. Hjelm, T. Ramos, "Sulfur Poisoning of SOFC Anodes: Effect of Overpotential on Long-Term Degradation", J. Electrochem. Soc. 161 (2014) F734–F743. doi:10.1149/2.080406jes.
6. A. Hagen, "Sulfur Poisoning of the Water Gas Shift Reaction on Anode Supported Solid Oxide Fuel Cells", J. Electrochem. Soc. 160 (2013) F111–F118. doi:10.1149/2.060302jes.
7. C. Graves, J. Hjelm, "Advanced impedance modeling of solid oxide electrochemical cells", in: Proc. of the 11th European SOFC and SOE Forum 2014, Lucerne, Switzerland, 2014: p. B1203.
8. R.R. Mosbæk, J. Hjelm, R. Barfod, P.V. Hendriksen, "Fuel flow distribution in SOFC stacks revealed by impedance spectroscopy", in: Proc. of the 11th European SOFC and SOE Forum 2014, Lucerne, Switzerland, 2014: p. A0902.

1.3.8.2 Poster / Oral Conference Presentations

1. "Resistivity and Interfacial Properties of CGO-YSZ bilayers in solid oxide fuel cells" J. Hjelm, P. Hjalmarsson, K. Brodersen, S. Foghmoes, poster presentation at the 222nd Meeting of the Electrochemical Society, Honolulu, HI, USA, October 7-12, 2012
2. "Impedance of SOFC Composite Electrodes", J.Nielsen, J. Hjelm, oral presentation at the 9th International Symposium on Electrochemical Impedance Spectroscopy (EIS2013), Okinawa Convention Center, Okinawa, Japan, June 16-21, 2013.
3. "Sulfur Poisoning of Ni/stabilized-zirconia Anodes – Effect on Long-Term Durability", A. Hauch, 13th International Symposium on Solid Oxide Fuel Cells (SOFC-XIII), Okinawa, Japan, October 6-11, 2013
4. "Process Specific Degradation Analysis of SOFCs " J. Hjelm, 11th International Symposium on Solid Oxide Fuel Cells (SOFC): Materials, Science and Technology, at 38th International Conference and Exposition on Advanced Ceramics and Composites, January 26-31, Daytona Beach, FL, United States
5. "Advanced impedance modeling of solid oxide electrochemical cells", C. Graves, oral presentation at the 11th European SOFC and SOE Forum 2014, Lucerne, Switzerland, 2014
6. "Fuel flow distribution in SOFC stacks revealed by impedance spectroscopy" R.R. Mosbæk, oral presentation at the 11th European SOFC and SOE Forum 2014, Lucerne, Switzerland, 2014

1.3.8.3 Patent Applications

1. "Cold Idle Operation of SOFC System" European application no. 14171742.1.

1.4 Utilization of Project Results

The Danish roadmap and strategy 2013-25 sets out the development targets necessary for commercialization of the Danish SOFC technology.[26] The results from the present project will play a key role in achieving these targets. The results, in particular improvements in cell components, performance, durability, improved understanding of degradation, diagnostic methods, and fruitful degradation mitigation strategies will be transferred to Topsoe Fuel Cell, in order to allow implementation in cells used in stacks and systems. A patent application and multiple scientific publications have already been produced as a direct result of the project. Furthermore, the results will be the basis for the necessary further research and development at DTU Energy Conversion and Topsoe Fuel Cell.

1.5 Project Conclusion and Perspective

The key outcome of the project can be summarized in the following points:

- Requirements and reasonable expectations on the demands on a SOFC system operating in a smart grid context was analyzed and although a Smart Grid does not exist yet, some important operating modes were suggested and examined in the project, leading to the conclusion that the SOFC technology is able to follow the expected dynamic load changes and that the overall characteristics of the SOFC technology makes it relevant for Smart Grid applications. However, it has also been evident that the biggest issues before successfully implementing the SOFC technology in Smart Grid systems relies on improvements of lifetime and robustness.
- Performance mapping of stacks and PowerCores with respect to the defined operating modes, various fuels and degrees of fuel utilization, and transient operation limits were investigated, and system DC efficiences of up to 65 %. "Power burst" operation can be realized but at a significant efficiency penalty.
- As durability and robustness are very important for the commercial success of the technology some of the effort in the project was refocused on a statistical analysis of observed failure modes in stacks, and at TOFC solutions to facilitate the identification, characterization, and quantification of lifetime limiting mechanisms using literature, component tests, physical characterization and stack post mortem analysis were established, with results added as categorized entries in a "Degradation Mechanisms Database".
- Leak testing of sealant gaskets in a custom component test set-up as a function of time and thermal cycles showed excellent results in air, and pointed to benefits of using slightly thicker glass sealant gaskets in the case of reducing atmosphere. Thermal cycling did not influence the leak tightness significantly.
- Further exploration of the influence of sulfur impurities in reformate fuel gas indicated that a critical anode polarization limit exists beyond which the cell stability decreases significantly.
- A screening study of potential anode cermet electrode surface coatings produced by infiltration of metal salts into the porous anode for improved impurity tolerance identified a single promising material (ceria) which could be recommended for future testing.
- Three different cells were characterized in reformate gas and hydrogen fuel. Detailed parameter dependencies were obtained, and process specific overpotential - current density curves were constructed from recorded impedance data. Such overpotential curves can be used as model input and for correlation of degradation to the overpotential of the electrodes during operation.
- Improved cells were produced using tape-casting and the use of thinner electrolyte layers and finer anode layers were shown to result in improved performance, as expected. The use of a large scale production technique provides a good platform for transfer of such results to industry.
- Durability testing at the single cell level was carried out in reformate gas and variations in the initial degradation (observed over 1000 h of operating time) is dependent on the fuel gas composition. In an internally reformed methane fuel mixture greater instantaneous degradation rates were observed after over the first 1000 h than in hydrogen fuel, but the overall degradation was approximately the same after 1000 h for the same cell type. Longer tests are needed to establish reliable long-term degradation rates of single cells.

[26] Strategi for udvikling af SOFC-brændselsceller 2013-2025, Partnerskabet for Brint og Brændselsceller, http://www.hydrogennet.dk/sofc-strategi1/

- Significant advances were made in the areas of data analysis, visualization, and interpretation with implementation of new advanced methods for impedance data analysis, and with the introduction of physically appropriate equivalent circuit models for porous electrodes.
- Implemented improvements in a recent production batch of stacks were shown to yield satisfactory results when tested in the project using a relatively harsh quality assurance test profile, indicating that the improvements lead to increased stack robustness.
- A method for spatially resolved measurements of temperature gradients using internal temperature probes were developed and demonstrated.
- Electrochemical impedance spectroscopy was successfully implemented and used to simultaneously record impedance spectra for a whole (14 cell) stack, and lead to new insight into fuel flow distribution throughout a stack, and provided information on the 1-D average cell temperature gradient from top to bottom of the stack.
- The adhesion properties of anode - interconnect steel, and cathode - interconnect steel interfaces was quantified using a three-point bending method, and the mechanical properties of materials and interfaces in the cell was investigated using nanoindentation. The weakest point was found to be the cathode - interconnect steel interface.
- Ink-jet deposition was shown to be a useful production technique for manufacturing of an electrolyte layer of only ~1.2 μm thickness.
- Methods for investigation of fundamental interactions (wetting and agglomeration) between Ni and a ceramic substrate were explored, and although in its infancy, and the results indicate a significantly different wetting and agglomeration behaviour on YSZ and ScYSZ, which is also influenced by impurities and grain orientation.

In this project, we gained significant new insight into smart grid relevant operating modes, and gained new knowledge about many different aspects that influences the lifetime of SOFC systems operated in a smart grid context. Robustness and durability are still some of the most important topics for commercial success of the technology. The cell components produced and investigated yields performance improvements that are in line with the objectives of the national SOFC development strategy. It is expected that many of the methods developed in this project for testing and analysis of cells, stacks, and components will be used in future projects and in this way accelerate the commercialization of the technology. Some of the questions raised in this project, for example the influence of transient operation, and operation in different modes on the single cell performance will be further explored in the project SOFC4RET. The degradation database created at TOFC will also be an important tool to guide future developments toward highly durable and robust SOFC systems. The outcome of this project provides guidelines for the future focus of development and research in order to achieve increased performance, improved diagnostics, better durability and robustness, and more cost-efficient anode-supported solid oxide fuel cell technology.